Semianalytical Geometry-Property Relationships for Some Generalized Classes of Pentamodelike Additively Manufactured Mechanical Metamaterials

R. Hedayati,[1,*] S. Jedari Salami,[2] Y. Li,[1] M. Sadighi,[3] and A.A. Zadpoor[4]

[1]*Novel Aerospace Materials group, Faculty of Aerospace Engineering, Delft University of Technology (TU Delft), Kluyverweg 1, 2629 HS, Delft, The Netherlands*
[2]*Department of Mechanical Engineering, Damavand branch, Islamic Azad University, Damavand, Iran*
[3]*Department of Mechanical Engineering, Amirkabir University of Technology (Tehran Polytechnic), Hafez Ave, Tehran, Iran*
[4]*Department of Biomechanical Engineering, Faculty of Mechanical, Maritime, and Materials Engineering, Delft University of Technology (TU Delft), Mekelweg 2, 2628 CD, Delft, The Netherlands*

We study a special class of mechanical metamaterials, namely lattices, based on beams (struts) with nonuniform cross sections, of which pentamode mechanical metamaterials are a special case. Five symmetric beam types including simple cylinder, concave double cone, convex double cone, concave hyperbolic, and convex hyperbolic are considered. Three types of loads including lateral force, axial force, and moment are applied to the free end of cantilever beams with the five aforementioned geometries and their responses are compared in terms of displacement, normal stress variation along the beam length, and shear stress variation along the beam length. Using the displacement diagrams obtained for different strut geometries and loading conditions, semi-analytical relationships are derived for the displacement at the end of cantilever beams. The semi-analytical relationships are then used to calculate the elastic modulus and yield strength of lattice structures based on two types of unit cells, namely diamond and cube. We also build numerical models and perform experiments to benchmark our semi-analytical results. Comparison of the analytical, numerical, and experimental results demonstrate the accuracy of the semi-analytical relationships presented for the mechanical properties of this class of mechanical metamaterials. Moreover, in both the cube- and diamond-based structures, increasing the α value (i.e., the ratio of the largest to the smallest cross-section radius in each strut) at a constant relative density decreases the elastic modulus, yield strength, the initial maximum stress, and the plateau stress.

I. INTRODUCTION

Metamaterials are engineered structures that are rationally designed to exhibit unusual physical properties. They are often called after the type of the physical property they target, for example, optical metamaterials [1,2], acoustic metamaterials [3,4], or mechanical metamaterials [5–8]. Mechanical metamaterials, in particular, aim at achieving unusual mechanical properties not readily found in nature such as negative Poisson's ratio [9–12], negative compressibility [13,14], ultrahigh stiffness [15], or negative elasticity [16,17]. The small-scale geometry of mechanical metamaterials determines the properties they exhibit at larger scales. Geometry-property relationships are, therefore, of utmost interest in the process of rationally designing mechanical metamaterials.

Geometries that are based upon beam-like elements (sometimes called struts) have been often used for development of mechanical metamaterials. In this approach, a number of struts are used to create a space-filling unit cell that is then repeated in different directions to create the microarchitecture of the metamaterial. One advantage of the geometries based on beam-like elements is that beam theories such as Euler-Bernoulli or Timoshenko can be used to derive analytical geometry-property relationships [18–20].

A natural extension of the geometries based on beams with constant cross sections is to allow for beams with variable cross sections. Milton and Cherkaev have shown in their seminal paper [21] that lattices based on beams with variable cross sections could be the basis for creating pentamode metamaterials. Pentamode metamaterials are a special class of extremal materials that exhibit unusually high resistance against deformations in certain directions (associated with the extremely large eigenvalues of the elasticity tensor), while being extremely compliant in some other directions (associated with the near-zero eigenvalues of the elasticity tensor). In the case of pentamode metamaterials, the extremely large and near-zero eigenvalues of the elasticity tensor translate to a very large

*r.hedayati@tudelft.nl; rezahedayati@gmail.com

bulk modulus and negligible shear modulus. That is why pentamode metamaterials are sometimes called metafluids [22,23]. More importantly, Milton and Cherkaev have shown that pentamode metamaterials can be used as a platform for realizing metamaterials with any thermodynamically admissible elasticity tensor [21]. Pentamode metamaterials were not manufactured until 2012 [24] when the availability of advanced additive manufacturing [three-dimensional (3D) printing] techniques allowed for their realization. Continued improvement of additive manufacturing techniques that allow for fabrication of metamaterials with arbitrarily complex geometries on one hand and the potential of pentamode-like metamaterials as a general platform for the design of mechanical metamaterials with any given elasticity tensor on the other hand highlight the importance of deriving analytical geometry-property relationships for lattices based on beams with variable cross sections.

An important barrier to deriving such relationships is that theories comparable with Euler-Bernoulli and Timoshenko do not exist for beams with variable cross sections. In this study, we take an analytical approach to derive an exact beam theory for certain classes of beams with variable cross sections. The considered types of variable cross sections include not only the type used in pentamode metamaterials (i.e., convex double cone) but also three other types (i.e., concave double cone, concave hyperbolic, and convex hyperbolic). In the next step, we use the presented beam theory to derive semi-analytical relationships for the mechanical properties of lattices based on the diamond and cubic unit cells. The geometry proposed by Milton and Cherkaev [21] for pentamode metamaterials (i.e., diamond-type lattices made from convex double-cone beams) are, thus, a special case of the lattices for which we provide semi-analytical relationships. We then compare the mechanical properties predicted by our semi-analytical relationships with the computational results obtained using finite element (FE) models. Finally, we use an additive manufacturing (3D printing) technique to fabricate specimens with the same type of lattice structures and two types of variable cross sections (convex double cone and concave double cone) as used in derivation of the semi-analytical relationships. The predictions of the semi-analytical relationships are then compared with the compressive mechanical properties observed for the additively manufactured specimens.

II. MATERIALS AND METHODS

A. Analytical and semi-analytical solutions

1. The geometrical relationships

In order to objectively compare the responses of the five different types of beams, they must have something in common. Since adjusting the elastic properties of mechanical metamaterials given their available mass is important

TABLE I. Formulas for cross-section radius z in different geometries.

	Left part	Right part
Cylinder	$z = r$	
Concave double cone	$z = \frac{2(r-R)}{l}x + R$	$z = \frac{2(R-r)}{l}x + (2r - R)$
Convex double cone	$z = \frac{2(R-r)}{l}x + r$	$z = \frac{2(r-R)}{l}x + (2R - r)$
Concave hyperbolic	$z = r + D - \left(D^2 - \left(x - \frac{l}{2}\right)^2\right)^{1/2}$	
	where $D = \frac{(R-r)^2 + \left(\frac{l}{2}\right)^2}{2(R-r)}$	
Convex hyperbolic	$z = D - R - \left(D^2 - \left(x - \frac{l}{2}\right)^2\right)^{1/2}$	
	where $D = \frac{(R-r)^2 + \left(\frac{l}{2}\right)^2}{2(R-r)}$	

in a large number of applications, we compare the response of the different types of beams while fixing their total mass. In all geometries, the ratio of the small radius to the beam length is denoted by β (i.e., $\beta = r/l$), while the ratio of the large radius to the small radius is denoted by α, that is, $\alpha = R/r$. Table I lists the cross-section radius, z, as a function of the distance from the strut edge, x, for the different geometries considered here. In conical geometries [Figs. 1(d) and 1(e)], the ratio β can be expressed as a function of geometrical dimensions and the volume occupied by the beam V_{strut} as

$$\beta = \left(\frac{3V_{\text{strut}}}{\pi l^3 (1 + \alpha + \alpha^2)}\right)^{1/2}. \quad (1)$$

In hyperbolic geometries, however, it is not possible to obtain a closed-form equation for β (which subsequently gives the smaller radius, r). The value of β must, therefore, be found using numerical methods such as Newton-Raphson. To do this, first a r_0 is guessed and the mass of the beam is calculated using

$$M_0 = \rho \int_0^l \pi z_0^2 dx, \quad (2)$$

where $z_0 = r_0 + D_0 - \{D_0^2 - [x - (l/2)]^2\}^{1/2}$ (according to Table I) and $D_0 = \{[(\alpha - 1)^2 r_0^2 + (l/2)^2]/[2r_0(\alpha - 1)]\}$. If the value of $M_0 - M$ is nonzero (where M is the given mass of the strut), a second guess is used for the smaller radius, r

$$r_1 = r_0 - \frac{f(r_0)}{f'(r_0)}, \quad (3)$$

where f is a function defined as $f(r_i) = M_i - M$ with

$$M_i = \rho \int_0^l \pi z_i^2 dx, \quad (4)$$

where $z_i = r_i + D_i - \{D_i^2 - [x - (l/2)]^2\}^{1/2}$ (according to Table I) and $D_i = \{[(\alpha - 1)^2 r_i^2 + (l/2)^2]/[2r_i(\alpha - 1)]\}$.
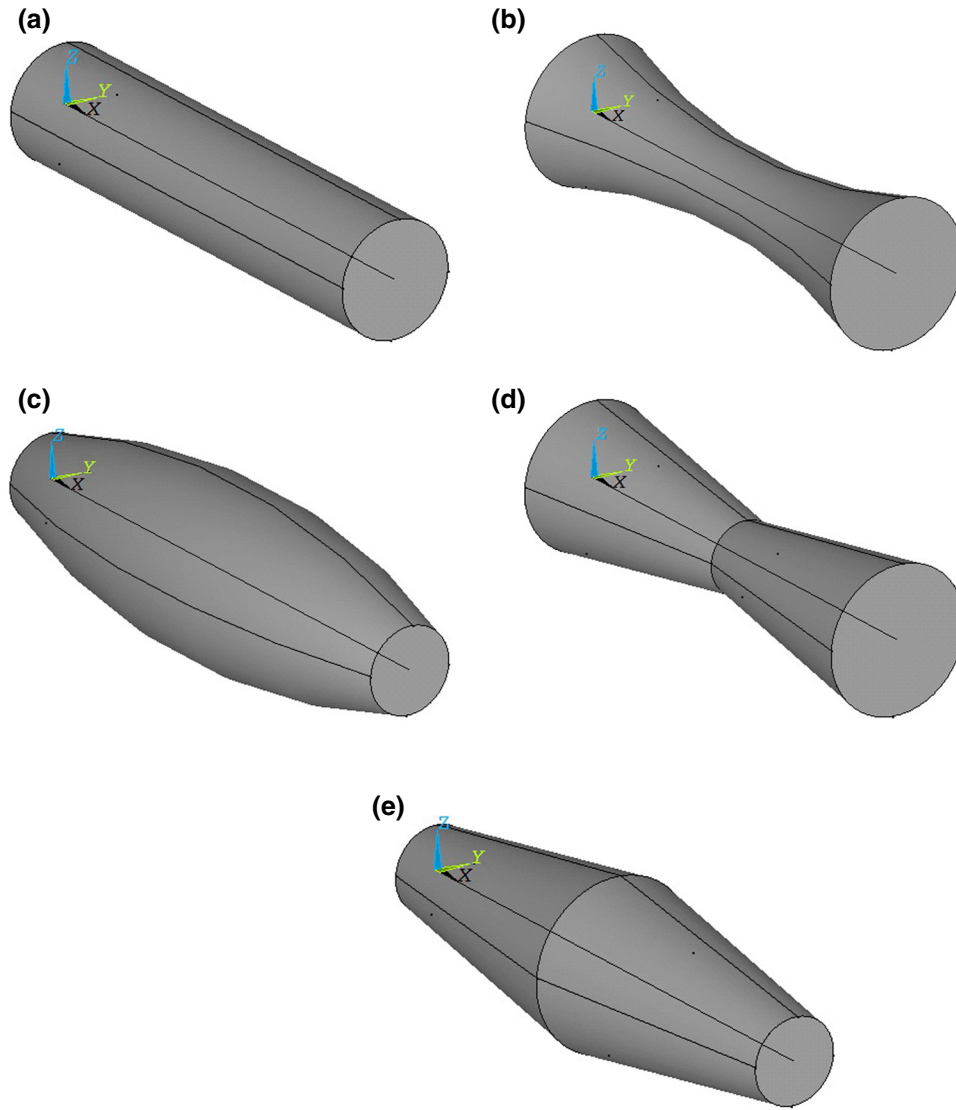
FIG. 1. Five beam geometries considered for analytical study: (a) simple cylinder, (b) concave hyperbolic, (c) convex hyperbolic, (d) concave double-cone, and (e) convex double-cone.

The process is repeated as

$$r_{n+1} = r_n - \frac{f(r_n)}{f'(r_n)}, \tag{5}$$

until a sufficiently accurate value is reached. For each α, a Newton-Raphson loop is used to find r, and thus, $R = \alpha r$.

2. Beams with variable cross sections

In the Timoshenko beam theory, the displacements of the different points of the beam in the x, y, and z directions are as follows:

$$u(x,y,z) = z\varphi(x) + u_0(x),$$
$$v(x,y,z) = 0,$$
$$w(x,y,z) = w(x), \tag{6}$$

where (x,y,z) represents the coordinates of a point in the beam (Fig. 1), φ is the angle of the rotation of the normal to the midsurface of the beam, u_0 is the displacement of the midsurface in the x direction, and w is the displacement of the midsurface in the z direction. The components of the strain tensor for a beam with linear strains are

$$\varepsilon_{xx} = \frac{\partial u}{\partial x} = z\frac{\partial \varphi}{\partial x} + \frac{\partial u_0}{\partial x},$$
$$\varepsilon_{zx} = \frac{\partial u}{\partial z} + \frac{\partial w}{\partial x} = \varphi + \frac{\partial w}{\partial x},$$
$$\varepsilon_{yy} = \varepsilon_{zz} = \gamma_{xy} = \gamma_{yz} = 0. \tag{7}$$

The corresponding stresses of the beam are, thus, given as

$$\sigma_{xx} = E_s\varepsilon_{xx} = E_s\left(\frac{\partial u_0}{\partial x} + z\frac{\partial \varphi}{\partial x}\right),$$

$$\tau_{zx} = \kappa G_s \varepsilon_{zx} = \kappa G_s \left(\varphi + \frac{\partial w}{\partial x} \right),$$

$$\sigma_{yy} = \sigma_{zz} = \tau_{xy} = \tau_{yz} = 0, \tag{8}$$

where E_s and G_s are the elastic and shear moduli of the material and κ is the Timoshenko's shear coefficient. We use the Ritz method to derive the governing equations of equilibrium from the total potential energy function of the beam. The total potential energy (Π) includes the strain energy (U) and the potential of external forces (W).

$$\Pi = U + W. \tag{9}$$

The strain energy of the sandwich beam that consists of energetically conjugate pairs of stress and strain is given by

$$U = \iiint \left[\int \sigma_{xx} d\varepsilon_{xx} + \int \sigma_{yy} d\varepsilon_{yy} + \int \sigma_{zz} d\varepsilon_{zz} \right.$$
$$\left. + \int \tau_{xy} d\gamma_{xy} + \int \tau_{yz} d\gamma_{yz} + \int \tau_{xz} d\gamma_{xz} \right] dV. \tag{10}$$

The strain energy expression may be obtained by substituting Eq. (8) into Eq. (10) and then integrating over the strain terms. The resulting relationship is as follows:

$$U = \frac{1}{2} \iiint \left[E_s \left(\frac{\partial u_0}{\partial x} + z \frac{\partial \varphi}{\partial x} \right)^2 + \kappa G_s \left(\varphi + \frac{\partial w}{\partial x} \right)^2 \right] dV,$$
$$= \frac{1}{2} \int_{x=0}^{l} \left[E_s A \left(\frac{\partial u_0}{\partial x} \right)^2 + E_s I \left(\frac{\partial \varphi}{\partial x} \right)^2 \right.$$
$$\left. + \kappa G_s A \left(-\varphi + \frac{\partial w}{\partial x} \right)^2 \right] dx. \tag{11}$$

The potential energy of external work is equal to

$$W = -\int_{x=0}^{l} [P_x u_0 + F_z w + M_{xy} \varphi] \delta_d(x - x_k) \, dx, \tag{12}$$

where P_x, F_z, and M_{xy} are the external axial and lateral concentrated loads and the concentrated bending moments applied to the beam at point $x = x_k$, respectively. In Eq. (12), $\delta_d(x - x_k)$ is the Dirac delta function at the location of the concentrated loads. The three variables w, φ, and u_0, could be written as the following summations

$$w = \sum_{i=1}^{\infty} W_i S_i^w,$$

$$\varphi = \sum_{i=1}^{\infty} \Phi_i S_i^\varphi,$$

$$u_0 = \sum_{i=1}^{\infty} U_i S_i^u, \tag{13}$$

where S_i^w, S_i^φ, S_i^u are, respectively, the lateral displacement, rotational, and axial shape functions that should satisfy the boundary conditions of the beam. Since the beams are cantilever, a good approximation for all the shape functions is

$$S_i^w = S_i^\varphi = S_i^u = \left(\frac{x}{l} \right)^i. \tag{14}$$

By substituting the shape functions into Eq. (13) and the obtained relationships into Eqs. (11) and (12), the total potential energy can be calculated as a function of the unknown displacement coefficients W_i, Φ_i, and U_i as

$$\Pi = \frac{1}{2} \int_{x=0}^{l} \left[E_s A \left(\sum U_i \frac{\partial S_i^u}{\partial x} \right)^2 + E_s I \left(\sum \Phi_i \frac{\partial S_i^\varphi}{\partial x} \right)^2 \right.$$
$$\left. + \kappa G_s A \left(\sum W_i \frac{\partial S_i^w}{\partial x} - \sum \Phi_i S_i^\varphi \right)^2 \right] dx$$
$$- \int_{x=0}^{l} \left[P_x \sum_{i=1}^{\infty} U_i S_i^u + F_z \sum_{i=1}^{\infty} W_i S_i^w \right.$$
$$\left. + M_{xy} \sum_{i=1}^{\infty} \Phi_i S_i^\varphi \right] \delta_d(x - x_k) \, dx. \tag{15}$$

In this study, only three concentrated loads $P_x = P$, $F_z = F$, and $M_{xy} = M$ at $x = l$ are considered. Finally, by inserting Eq. (9) into the generalized Lagrange equations, the governing equations of the problem are obtained as

$$\frac{\partial \Pi}{\partial W_i} = 0 \rightarrow \int_{x=0}^{l} \kappa G_s A \sum_{k=1}^{\infty} \left(W_k \frac{\partial S_k^w}{\partial x} - \Phi_k S_k^\varphi \right) \frac{\partial S_i^w}{\partial x} dx$$
$$- \int_{x=0}^{l} \sum_{i=1}^{\infty} F S_i^w \delta_d(x - x_k) \, dx = 0,$$

$$\frac{\partial \Pi}{\partial \Phi_i} = 0 \rightarrow \int_{x=0}^{l} E_s I \sum_{k=1}^{\infty} \left(\Phi_k \frac{\partial S_k^\varphi}{\partial x} \right) \frac{\partial S_i^\varphi}{\partial x} dx$$
$$- \int_{x=0}^{l} \kappa G_s A \sum_{k=1}^{\infty} \left(W_k \frac{\partial S_k^w}{\partial x} - \Phi_k S_k^\varphi \right) S_i^\varphi dx$$
$$- \int_{x=0}^{l} \sum_{i=1}^{\infty} M S_i^\varphi \delta_d(x - x_k) dx = 0,$$

$$\frac{\partial \Pi}{\partial U_i} = 0 \rightarrow \int_{x=0}^{l} E_s A \sum_{k=1}^{\infty} \left(U_k \frac{\partial S_k^U}{\partial x} \right) \frac{\partial S_i^U}{\partial x} dx$$
$$- \int_{x=0}^{l} \sum_{i=1}^{\infty} P S_i^U \delta_d(x - x_k) dx = 0. \tag{16}$$

Therefore,

$$\begin{bmatrix} \left[\int_0^l \kappa G_s A \dfrac{\partial S_i^w}{\partial x} \dfrac{\partial S_j^w}{\partial x} dx \right]_{N \times N} & \left[-\int_0^l \kappa G_s A \dfrac{\partial S_i^w}{\partial x} S_j^\varphi dx \right]_{N \times N} & [0]_{N \times N} \\[2em] \left[-\int_0^l \kappa G_s A \, S_i^\varphi \dfrac{\partial S_j^w}{\partial x} dx \right]_{N \times N} & \left[\int_0^l E_s I \dfrac{\partial S_i^\varphi}{\partial x} \dfrac{\partial S_j^\varphi}{\partial x} dx + \int_0^l \kappa G_s A \, S_i^\varphi \, S_j^\varphi dx \right]_{N \times N} & [0]_{N \times N} \\[2em] [0]_{N \times N} & [0]_{N \times N} & \left[\int_0^l E_s A \dfrac{\partial S_i^U}{\partial x} \dfrac{\partial S_j^U}{\partial x} dx \right]_{N \times N} \end{bmatrix}_{3N \times 3N}$$

$$\times \begin{Bmatrix} W_1 \\ W_2 \\ \vdots \\ W_N \\ \Phi_1 \\ \Phi_2 \\ \vdots \\ \Phi_N \\ U_1 \\ U_2 \\ \vdots \\ U_N \end{Bmatrix}_{2N \times 1} = \begin{Bmatrix} F_1 \\ F_2 \\ \vdots \\ F_N \\ M_1 \\ M_2 \\ \vdots \\ M_N \\ P_1 \\ P_2 \\ \vdots \\ P_N \end{Bmatrix}_{3N \times 1} , \quad \text{for} \quad i,j = 1, \ldots, N \tag{17}$$

By multiplying both sides of Eq. (17) by the inverse of the stiffness matrix, the coefficients W_i, Φ_i, and U_i for $i = 1, \ldots, N$ are calculated. Having obtained the coefficients, the lateral displacement, rotation, and axial displacement of the free end of the beam are given as

$$\delta_{\text{lateral}} = \sum_{k=1}^N W_i,$$

$$\theta = \sum_{k=1}^N \Phi_i,$$

$$\delta_{\text{axial}} = \sum_{k=1}^N U_i. \tag{18}$$

A MATLAB (Mathworks, USA) code is written to determine the end displacements and rotations for beams with variable cross sections. All the beams (in both the analytical and numerical solutions) have identical masses of $m_0 = 0.003$ kg and lengths of $l_0 = 0.05$ m. The α values are changed from 1 to 6 to study the effects of the α value on the displacement, normal stress, and shear stress diagrams. The material properties of steel are introduced into the problem $\rho_0 = 7800$ kg/m^3, $E_{s,0} = 200$ GPa, $G_{s,0} = 79.3$ GPa, and $\nu_{s,0} = 0.3$. The amount of the applied forces and moments are chosen in such a way that the maximum value of displacement does not exceed 0.01 m. For axial force loading, lateral force loading, and moment loading,

$F_0 = 0.1$ N, $M_0 = 0.002$ N m, and $P_0 = 1000$ N are used, respectively.

For the special case of double-cone struts under an axial load, it is also possible to obtain closed-form equations. For a truncated cone with the length $l/2$, smaller diameter r, and larger diameter R, the axial expansion/contraction under axial force P can be found as:

$$\delta_{\text{axial}} = \frac{Pl}{2\pi E_s} \frac{1}{(R-r)} \int_r^R \frac{dr}{r^2} = \frac{Pl}{2\pi E_s rR} = \frac{Pl}{2\pi E_s \alpha r^2}. \tag{19}$$

3. Elastic modulus of metamaterials and lattice structures

Obtaining closed-form solutions for beams with variable cross sections is not possible. In this study, we first obtain analytical results for struts with different geometries and with the specifications described in the last paragraph. Cubic curves are then fitted to the displacements vs α diagrams of the ends of cantilever beams with different geometries under different loading conditions. All the fitted curves have the following form

$$\delta = C \left(\frac{E_{s,0}}{E_s} \right) \sum_{i=1}^N (p_i \alpha^{N-i}), \tag{20}$$

where C depends on the loading condition and $p_1 - p_N$ depends on both the loading condition and strut geometry. In this study, $N = 4$ terms are used for

TABLE II.   Constants of the lateral and axial displacement of the struts with different geometries under different loading conditions. For our case study, the following parameters are used: $m_0 = 0.003$ kg, $\rho_0 = 7800$ kg/m^3, $l_0 = 0.05$ m, $F_0 = 0.1N$, $M_0 = 0.002$ N m, and $P_0 = 1000N$.

	C	p_1	p_2	p_3	p_4
Double-cone concave (Lateral force, F)	$\dfrac{F}{F_0}\left(\dfrac{m_0}{\rho_0 V_{\text{strut}}}\right)^2\left(\dfrac{l}{l_0}\right)^5$	-1.4647×10^{-7}	2.1585×10^{-6}	-3.9025×10^{-6}	6.3701×10^{-6}
Double-cone concave (Moment, M)	$\dfrac{M}{M_0}\left(\dfrac{m_0}{\rho_0 V_{\text{strut}}}\right)^2\left(\dfrac{l}{l_0}\right)^4$	-1.0391×10^{-7}	1.5521×10^{-6}	-2.4348×10^{-6}	3.6896×10^{-6}
Double-cone concave (Axial force, P)	$\dfrac{P}{P_0}\left(\dfrac{m_0}{\rho_0 V_{\text{strut}}}\right)^2\left(\dfrac{l}{l_0}\right)^2$	-1.7731×10^{-7}	2.099×10^{-6}	1.2912×10^{-6}	2.855×10^{-5}
Double-cone convex (Lateral force, F)	$\dfrac{F}{F_0}\left(\dfrac{m_0}{\rho_0 V_{\text{strut}}}\right)^2\left(\dfrac{l}{l_0}\right)^5$	2.0963×10^{-7}	9.8763×10^{-7}	-2.8271×10^{-7}	3.2737×10^{-6}
Double-cone convex (Moment, M)	$\dfrac{M}{M_0}\left(\dfrac{m_0}{\rho_0 V_{\text{strut}}}\right)^2\left(\dfrac{l}{l_0}\right)^4$	7.2524×10^{-8}	5.8636×10^{-7}	-5.5547×10^{-7}	2.4354×10^{-6}
Double-cone convex (Axial force, P)	$\dfrac{P}{P_0}\left(\dfrac{m_0}{\rho_0 V_{\text{strut}}}\right)^2\left(\dfrac{l}{l_0}\right)^2$	-1.7033×10^{-7}	2.2245×10^{-6}	8.2452×10^{-7}	2.8861×10^{-5}
Hyperbolic concave (Lateral force, F)	$\dfrac{F}{F_0}\left(\dfrac{m_0}{\rho_0 V_{\text{strut}}}\right)^2\left(\dfrac{l}{l_0}\right)^5$	2.916×10^{-7}	-2.5066×10^{-7}	1.3737×10^{-6}	2.4735×10^{-6}
Hyperbolic concave (Moment, M)	$\dfrac{M}{M_0}\left(\dfrac{m_0}{\rho_0 V_{\text{strut}}}\right)^2\left(\dfrac{l}{l_0}\right)^4$	2.1674×10^{-7}	-1.0061×10^{-7}	8.1761×10^{-7}	1.551×10^{-6}
Hyperbolic concave (Axial force, P)	$\dfrac{P}{P_0}\left(\dfrac{m_0}{\rho_0 V_{\text{strut}}}\right)^2\left(\dfrac{l}{l_0}\right)^2$	-2.0847×10^{-7}	3.5759×10^{-6}	-1.888×10^{-6}	3.031×10^{-5}
Hyperbolic convex (Lateral force, F)	$\dfrac{F}{F_0}\left(\dfrac{m_0}{\rho_0 V_{\text{strut}}}\right)^2\left(\dfrac{l}{l_0}\right)^5$	7.0372×10^{-7}	-2.8385×10^{-6}	9.6897×10^{-6}	-4.2156×10^{-6}
Hyperbolic convex (Moment, M)	$\dfrac{M}{M_0}\left(\dfrac{m_0}{\rho_0 V_{\text{strut}}}\right)^2\left(\dfrac{l}{l_0}\right)^4$	6.6052×10^{-9}	1.2554×10^{-6}	-2.1702×10^{-6}	3.5615×10^{-6}
Hyperbolic convex (Axial force, P)	$\dfrac{P}{P_0}\left(\dfrac{m_0}{\rho_0 V_{\text{strut}}}\right)^2\left(\dfrac{l}{l_0}\right)^2$	-1.5939×10^{-7}	1.9506×10^{-6}	1.2663×10^{-6}	2.8809×10^{-5}

fitting and the obtained constants for different geometries and loading conditions are listed in Table I (for steel). The coefficient $(E_{s,0}/E_s)$ in Eq. (20) takes into account the change in the displacement due to the change in the elastic modulus of the bulk material when the bulk material has an elastic modulus other than $E_{s,0}$. The coefficient C is $(F/F_0)(m_0/\rho_0 V_{\text{strut}})^2(l/l_0)^5$, $(M/M_0)(m_0/\rho_0 V_{\text{strut}})^2(l/l_0)^4$, and $(P/P_0)(m_0/\rho_0 V_{\text{strut}})(l/l_0)^2$ for the lateral force, moment, and axial force, respectively (Table II). The steps needed for derivation of C factors can be found in the electronic supplementary material accompanying the paper [25]. Subsequently, we use the semi-analytical relationships given in Eq. (20) to obtain the elastic modulus of lattice structures with cubic and diamond unit cell types. The diamond unit cell is chosen due to the fact that the pentamode mechanical metamaterials proposed by Milton and Cherkaev [21] are based on the diamond unit cell. Since additive manufacturing of horizontal struts can be quite challenging not only in the powder bed fusion processes [26], but, as we will see later, also in material extrusion techniques, the cubic unit cell is chosen to highlight the manufacturability aspects.

Cube: For the structures based on the cubic unit cell, the vertical struts go under simple compression. If the total load P is applied to each unit cell, each vertical strut goes under the compressive load, P. The elastic modulus of each unit cell is obtained by $E_{\text{u.c.}} = Pl_{\text{u.c.}}/(A_{\text{u.c.}}\delta_{\text{u.c.}})$, where $l_{\text{u.c.}} = l$ is the dimension of the unit cell, $A_{\text{u.c.}}$ is the cross-section area of the unit cell, and $\delta_{\text{u.c.}}$ is the resulting displacement, which is equal to the displacement of the vertical strut δ_{axial}. Therefore, $E_{\text{u.c.}} = P/(l\delta_{\text{axial}})$, where δ_{axial} for each strut type is given in Eq. (20). The semi-analytical formula for elastic modulus of the cubic structure is, therefore, given as

$$\frac{E_{\text{u.c.}}}{E_s} = \frac{P_o}{E_{s,0}l\left(\dfrac{m_0}{\rho_0 V_{\text{strut}}}\right)\left(\dfrac{l}{l_0}\right)^2 \sum_{i=1}^{N}\left(p_i \alpha^{N-i}\right)}, \quad (21)$$

where the constant $p_1 - p_N$ is given in Table I for each strut geometry. In the cubic structure, $V_{\text{strut}} = V_{\text{mat}}/3$, where V_{mat} is the volume occupied by the material in each unit cell and is equal to $V_{\text{mat}} = \mu l^3$, where μ is the relative density of the structure, which is defined as the ratio of the volume occupied by the material inside a unit cell V_{mat} to the total volume occupied by the unit cell. Introducing

$V_{\text{strut}} = \mu l^3 / 3$ in Eq. (21) and simplifying gives

$$\left(\frac{E_{\text{u.c.}}}{E_s}\right)_{\text{cube}} = \frac{P_0 \rho_0 \mu l_0^2}{3 E_{s,0} m_0 \sum_{i=1}^{N} (p_i \alpha^{N-i})}, \qquad (22)$$

with $p_1 - p_N$ given either in the third or the sixth row of Table II (that correspond to the axial force constants of, respectively, concave double-cone and convex double-cone geometries).

Using Eq. (19), we can also obtain the closed-form analytical relationship for the elastic modulus of cubic structures with double-cone struts. By inserting $V_{\text{strut}} = \mu l^3 / 3$ in Eq. (1) and squaring both sides of the equation, we have

$$\beta^2 = \frac{\mu}{\pi(1 + \alpha + \alpha^2)}. \qquad (23)$$

By replacing $\beta = r/l$ in Eq. (23), we have

$$\frac{1}{r^2} = \frac{\pi(1 + \alpha + \alpha^2)}{\mu l^2}. \qquad (24)$$

Substituting Eq. (24) into Eq. (19) gives the displacement in a truncated single-cone strut with length $l/2$ as

$$\delta_{\text{TC}} = \frac{P(1 + \alpha + \alpha^2)}{2 E_s \alpha \mu l}. \qquad (25)$$

The displacement equation in a cubic unit cell is $\delta_{\text{u.c.}} = P_{\text{u.c.}} l_{\text{u.c.}} / (A_{\text{u.c.}} E_{\text{u.c.}})$. By setting $A_{\text{u.c.}} = l_{\text{u.c.}}^2 = l^2$, $P_{\text{u.c.}} = P$, and $\delta_{\text{u.c.}} = 2\delta_{\text{TC}}$ (note that each strut in a pentamode-like cubic structure is double cone rather than a single truncated cone), we have

$$E_{\text{u.c.}} = \frac{P}{2l\delta_{\text{TC}}} = \frac{\alpha\mu}{(1 + \alpha + \alpha^2)}. \qquad (26)$$

Diamond: If the external force P is applied to a structure based on the diamond unit cell, there is no difference between the loads transferred to the different struts of the unit cell due to the symmetry [Fig. 2(a)]. Therefore, we consider only one of the struts of the unit cell, for example AB [Fig. 2(b)]. Strut AB carries $P_{\text{AB}} = P/4$. The vertical force P_{AB} can be decomposed into axial force $P_{\text{AB,axial}} = (P/4) \sin\theta$ and lateral force $P_{\text{AB,lateral}} = (P/4) \cos\theta$ components, where $\theta = 35.26°$ [Fig. 2(c)]. Due to the symmetry present between vertex A of strut AB and the corresponding strut in the neighboring unit cell, vertex A must not rotate. Similarly, due to the symmetry between struts AB and BC, vertex B of strut AB cannot undergo any rotation. Therefore, strut AB can be considered as a cantilever beam at the end of which a lateral force, an axial force, and a bending moment are applied. In the case of a uniform cross-section area of the struts, the rotation caused by lateral force and the moment should be the same with opposite signs. Equation $P_{\text{AB}} l^2 / (2EI) = M_A l / (EI)$ can then be used to determine the bending moment as $M_A = (1/2) P_{\text{AB}} l \cos\theta$ [27]. In the case of struts with nonuniform cross sections, the noted equality does not hold. We, therefore, need to introduce a coefficient γ, where γ should be obtained for each case. Therefore, for the diamond structure with double-cone struts (i.e., $\alpha \neq 1$), we have $M_A = \gamma(1/2) P_{\text{AB}} l \cos\theta = \gamma(P/8) l \cos\theta$. The total vertical displacement of the free end of strut AB is

$$\delta_{\text{AB,vertical}} = \delta_{\text{AB},P,\text{axial}} \sin\theta + \delta_{\text{AB},P,\text{lateral}} \cos\theta - \delta_{\text{AB},M} \cos\theta, \qquad (27)$$

where $\delta_{\text{AB},P,\text{axial}}$ is the axial displacement in the strut due to the axial load $P_{\text{AB,axial}}$, $\delta_{\text{AB},P,\text{lateral}}$ is the lateral displacement due to the lateral force $P_{\text{AB,lateral}}$, and $\delta_{\text{AB},M}$ is the lateral displacement due to the moment M_A. Substituting Eq. (20) into Eq. (27) and by considering the coefficients given in Table II, the total displacement is

$$\delta_{\text{AB,vertical}} = \frac{E_{s,0}}{E_s} \left\{ \left[\frac{P_{\text{AB,axial}}}{P_0} \left(\frac{m_0}{\rho_0 V_{\text{strut}}}\right) \left(\frac{l}{l_0}\right)^2 \right] (\sin\theta) \sum_{i=1}^{N} (p_i \alpha^{N-i})_{\text{force, axial}} + \left[\frac{P_{\text{AB,lateral}}}{F_0} \left(\frac{m_0}{\rho_0 V_{\text{strut}}}\right)^2 \left(\frac{l}{l_0}\right)^5 \right] \right.$$
$$\left. \times (\cos\theta) \sum_{i=1}^{N} (p_i \alpha^{N-i})_{\text{force,lateral}} - \left[\frac{M_A}{M_0} \left(\frac{m_0}{\rho_0 V_{\text{strut}}}\right)^2 \left(\frac{l}{l_0}\right)^4 \right] (\cos\theta) \sum_{i=1}^{N} (p_i \alpha^{N-i})_{\text{moment}} \right\}, \qquad (28)$$

where the subscript p_i of $\sum_{i=1}^{N} (p_i \alpha^{N-i})$ in each of the three terms can be extracted from the corresponding row of Table II. Replacing $P_{\text{AB,axial}} = (P/4) \sin\theta$, $P_{\text{AB,lateral}} = (P/4) \cos\theta$, and $M_A = \gamma(P/8) l \cos\theta$ in Eq. (28) gives

$$\delta_{\text{AB,vertical}} = \frac{E_{s,0}}{E_s} \left\{ \left[\frac{\frac{P}{4} \sin^2\theta}{P_0} \left(\frac{m_0}{\rho_0 V_{\text{strut}}}\right) \left(\frac{l}{l_0}\right)^2 \right] \sum_{i=1}^{N} (p_i \alpha^{N-i})_{\text{force, axial}} + \left[\frac{\frac{P}{4} \cos^2\theta}{F_0} \left(\frac{m_0}{\rho_0 V_{\text{strut}}}\right)^2 \left(\frac{l}{l_0}\right)^5 \right] \right.$$
$$\left. \times \sum_{i=1}^{N} (p_i \alpha^{N-i})_{\text{force,lateral}} - \left[\frac{\gamma \frac{P}{8} l \cos^2\theta}{M_0} \left(\frac{m_0}{\rho_0 V_{\text{strut}}}\right)^2 \left(\frac{l}{l_0}\right)^4 \right] \sum_{i=1}^{N} (p_i \alpha^{N-i})_{\text{moment}} \right\}. \qquad (29)$$

Since the diamond unit cell has 16 struts, $V_{strut} = V_{mat}/16$ and $V_{mat} = \mu \, l_{u.c.}^3$. Therefore, $V_{strut} = \mu \, l_{u.c.}^3/16$. Similar to the cubic structure, the elastic modulus of each unit cell is obtained as $E_{u.c.} = Pl_{u.c.}/A_{u.c.}\delta_{u.c.}$. For the diamond unit cell, $l_{u.c.} = 2\sqrt{2}l\cos\theta$, $A_{u.c.} = l_{u.c.}^2$, and $\delta_{u.c.} = 4\delta_{AB,vertical}$. Therefore, $E_{u.c.} = \frac{P}{4\, l_{u.c.}\delta_{AB,vertical}}$, which, after inserting in Eq. (29), gives

$$E_{u.c.} = \frac{1}{l_{u.c.}\lambda} \frac{E_s}{E_{s,0}}, \tag{30}$$

with

$$\lambda = \left[\frac{\sin^2\theta}{P_0}\left(\frac{16m_0}{\rho_0\mu l_{u.c.}^3}\right)\left(\frac{l}{l_0}\right)^2\right]\sum_{i=1}^{N}(p_i\alpha^{N-i})_{force,\,axial}$$
$$+ \left[\frac{\cos^2\theta}{F_0}\left(\frac{16m_0}{\rho_0\mu l_{u.c.}^3}\right)^2\left(\frac{l}{l_0}\right)^5\right]\sum_{i=1}^{N}(p_i\alpha^{N-i})_{force,\,lateral}$$
$$- \left[\gamma\frac{l\cos^2\theta}{2M_0}\left(\frac{16m_0}{\rho_0\mu l_{u.c.}^3}\right)^2\left(\frac{l}{l_0}\right)^4\right]\sum_{i=1}^{N}(p_i\alpha^{N-i})_{moment}, \tag{31}$$

with $p_1 - p_N$ given in Table II. Since the coefficients p_i correspond to the curves obtained for the struts made of stainless steel, the relative elastic modulus of the structure for any given material is obtained as

$$\left(\frac{E_{u.c.}}{E_s}\right)_{diamond} = \frac{1}{l_{u.c.}\lambda E_{s,0}}. \tag{32}$$

The coefficient β for the diamond unit cell can be obtained by inserting $V_{strut} = \mu l_{u.c.}^3/16$ into Eq. (1), which gives

$$\beta = \left(\frac{3\sqrt{2}\mu\cos^3\theta}{\pi\,(1+\alpha+\alpha^2)}\right)^{1/2}. \tag{33}$$

4. Yield strength of metamaterials

To obtain the yield stress, first the normal and shear stresses in the critical points of the struts generated by axial force, lateral force, and moment are determined. It must be noted that yielding in the struts occurs at the point with the minimum cross-section area $A_r = \pi r^2 = \pi\beta^2l^2$. By replacing β from Eq. (1), we have

$$A_r = \pi\beta^2l^2 = \frac{3V_{strut}}{l(1+\alpha+\alpha^2)}. \tag{34}$$

Cube: For the cubic structure under compression, each strut goes under load P, and $V_{strut} = \mu l^3/3$. Therefore, the maximum stress in the struts equals the stress at the point with minimum cross-section area. As the cube-based structure consists of concave double-cone struts, the minimum cross-section area is at the middle point of each strut, and therefore, the initial plastic zone appears at $x = l/2$.

By replacing $V_{strut} = \mu l^3/3$ in $\sigma_{max} = P/A_r$, we have:

$$\sigma_{max} = \frac{(1+\alpha+\alpha^2)P}{\mu l^2}. \tag{35}$$

When the stress applied on the lattice structure P/l^2 reaches σ_Y, the maximum local stress in the struts $\{[(1+\alpha+\alpha^2)P]/\mu l^2\}$ equals $\sigma_{Y,s}$. A simple cross multiplication gives

$$\sigma_Y = \frac{\frac{\sigma_{Y,s}P}{l^2}}{\frac{(1+\alpha+\alpha^2)P}{\mu l^2}} = \frac{\sigma_{Y,s}\mu}{(1+\alpha+\alpha^2)}, \tag{36}$$

or

$$\frac{\sigma_Y}{\sigma_{Y,S}} = \frac{\mu}{(1+\alpha+\alpha^2)}. \tag{37}$$

Diamond structure with convex double-cone struts: As demonstrated in Figs. 7 and 8 in Sec. III A 3, both the normal and shear stresses in the beam with convex double-cone geometry reach their maximum value at $x = 0$ under both lateral force F [Figs. 7(a) and 8(a)] and moment M [Figs. 7(b) and 8(b)]. The maximum normal stress generated by the normal force P also occurs at $x = 0$ as the beam has the lowest cross-section area at that point.

For the diamond unit cell with convex double-cone struts, the normal force, the lateral force, and the momentum in the strut are $(P/4)\sin\theta$, $(P/4)\cos\theta$, and $\gamma(P/8)l\cos\theta$, respectively, where $\gamma = 0.7$ for $\mu = 0.1$ and $\gamma = 0.56$ for $\alpha = 2$. Therefore, the normal stress generated by the axial force at the root of the struts is given by

$$\sigma_{n,A} = \frac{P\sin\theta}{4A_r} = \frac{\frac{P\sin\theta}{4}}{\frac{3V_{strut}}{l(1+\alpha+\alpha^2)}} = \frac{Pl(1+\alpha+\alpha^2)\sin\theta}{12V_{strut}}$$
$$= \frac{(1+\alpha+\alpha^2)P\sin\theta}{4\mu l^2}. \tag{38}$$

The stress generated by the bending stress is

$$\sigma_{n,B} = \frac{Mr}{I} = \frac{Mr}{\frac{\pi}{4}r^4} = \frac{4M}{\pi r^3} = \frac{4\left(\gamma\frac{P}{8}l\cos\theta\right)}{\pi(\beta^3l^3)}$$
$$= \frac{(\gamma P\cos\theta)}{2\pi(\beta^3l^2)} = \frac{\gamma P\cos\theta}{2\pi l^2\left(\frac{3}{\pi l^3}\frac{V_{strut}}{(1+\alpha+\alpha^2)}\right)^{3/2}}. \tag{39}$$

For a diamond unit cell with double-cone struts, $V_{\text{strut}} = \left[\left\{\mu\left(2\sqrt{2}l\cos\theta\right)^3\right\}/16\right]$. Therefore:

$$\sigma_{n,B} = \frac{\gamma P \cos\theta}{2\pi l^2 \left(\frac{3\sqrt{2}\mu\ (\cos\theta)^3}{\pi(1+\alpha+\alpha^2)}\right)^{3/2}}$$

$$= \frac{\gamma P \cos\theta}{2\pi l^2}\left(\frac{\pi(1+\alpha+\alpha^2)}{3\sqrt{2}\mu\ (\cos\theta)^3}\right)^{3/2}. \tag{40}$$

The normal stress in the beam is the sum of both normal stresses, that is, $\sigma_{xx} = \sigma_{n,B} + \sigma_{n,A}$. On the other hand, the maximum shear stress generated by the lateral force is

$$\tau_{zx} = \frac{4}{3}\tau_{\text{ave, }zx} = \frac{4}{3}\frac{P}{4}\frac{\cos\theta}{A_r} = \frac{P}{3}\frac{l(1+\alpha+\alpha^2)\cos\theta}{3V_{\text{strut}}}$$

$$= \frac{16P}{9}\frac{l(1+\alpha+\alpha^2)\cos\theta}{\mu\left(2\sqrt{2}\ l\ \cos\theta\right)^3}, = \frac{\sqrt{2}}{18}\frac{(1+\alpha+\alpha^2)P}{\mu l^2 \cos\theta}. \tag{41}$$

As noted in Eq. (8), the other stress components in the von-Mises yield stress are neglected. Considering the axial normal stress (σ_{xx}) and transverse shear stress (τ_{zx}) components of stress, the von-Misses stress can be obtained as follows:

$$\sigma_V = \sqrt{(\sigma_{n,A}+\sigma_{n,B})^2 + 3\tau_{zx}^2}. \tag{42}$$

When the stress applied on the lattice structure $P/l_{\text{u.c.}}^2$ reaches σ_Y (i.e., the lattice structure yields), the maximum local stress in the struts σ_V equals $\sigma_{Y,s}$. A simple cross multiplication gives

$$\sigma_Y = \frac{P\sigma_{Y,S}}{l_{\text{u.c.}}^2\ \sigma_V}, \tag{43}$$

or

$$\frac{\sigma_Y}{\sigma_{Y,S}} = \frac{P}{8l^2\cos^2\theta\sqrt{(\sigma_{n,B}+\sigma_{n,A})^2 + 3\tau_{zx}^2}}, \tag{44}$$

with $\sigma_{n,A}$, $\sigma_{n,B}$, and τ_{zx} given in Eqs. (38), (40), and (41).

Diamond structure with concave double-cone struts: As demonstrated in Figs. 7 and 8, both the normal and shear stresses in the beam with concave double-cone geometry reach their maximum value at $x = l/2$ under both lateral force F [Figs. 7(a) and 8(a)] and moment M [Figs. 7(b) and 8(b)]. The maximum normal stress generated by normal force P also occurs at $x = l/2$ as the beam has the lowest cross-section area at the middle point. Therefore, the initial appearance of a plastic zone could be expected at $x = l/2$ for each strut.

For the diamond unit cell with concave double-cone struts, the normal force, lateral force, and momentum in the strut are, respectively, $(P/4)\sin\theta$, $(P/4)\cos\theta$, and $\gamma(P/8)l\cos\theta$, where $\gamma = 0.84$ for $\mu = 0.1$ and $\gamma = 0.7$ for $\alpha = 2$. Therefore, the stress generated by the normal force in the middle of the struts is the same as the stress at the root of the convex double-cone structure [i.e., Eq. (38)].

The stress generated by the bending stress is

$$\sigma_{n,B} = \frac{Mr}{I} = \frac{Mr}{\frac{\pi}{4}r^4} = \frac{4M}{\pi r^3} = \frac{4\left(\gamma\frac{P}{8}\frac{l}{2}\cos\theta\right)}{\pi(\beta^3l^3)}$$

$$= \frac{\gamma P \cos\theta}{4\pi l^2}\left(\frac{\pi(1+\alpha+\alpha^2)}{3\sqrt{2}\mu\ (\cos\theta)^3}\right)^{3/2}. \tag{45}$$

Similar to what was seen before, the total normal stress in the beam is given by $\sigma_{xx} = \sigma_{n,B} + \sigma_{n,A}$.

The maximum shear stress generated by the lateral force is the same as the one presented for the convex double-cone beam geometry [i.e., Eq. (41)]. Therefore, for the case of a concave double-cone, Eq. (44) can also be used as long as Eq. (45) is used for $\sigma_{n,B}$ instead of Eq. (40).

Buckling: In order to study the likelihood of the instability of struts (beams) under axial compressive loads applied at the free end of the beams, the Euler's critical load should be determined for each beam. According to this criterion, the critical load is the maximum load that a beam (strut) can bear without experiencing instability. The major load applied on the struts of diamond pentamode structures is bending as also demonstrated by the deformation of the lattice structure during the whole compression procedure.

For the cubic structure, however, the main type of loading is axial compression, which could lead to buckling instability. In the cube-based lattice structures, we have

$$P_{\text{cr}} = \frac{\pi^2 E_s I_r}{(L_e)^2} = \frac{\pi^2 E_s I_r}{4l^2}, \tag{46}$$

where P_{cr} is the Euler's critical load, E_s is the elastic modulus of the material from which the struts are made, I_r is the minimum area moment of inertia of the cross section of the strut, and L_e is the effective length of the struts. Since the axial load is applied to the end of the cantilever beam, the effective length equals $L_e = 2l$. Therefore,

$$\sigma_{\text{cr}} = \frac{\pi^2 E_s I_r}{4A_r l^2} = \frac{\pi^2 E_s r^2}{16\ l^2} = \frac{\pi^2 E_s \beta^2}{16}$$

$$= \frac{\pi^2 E_s}{16}\frac{3V_{\text{strut}}}{\pi l^3(1+\alpha+\alpha^2)} = \frac{\pi E_s}{16}\frac{\mu}{(1+\alpha+\alpha^2)}. \tag{47}$$

Consequently,

$$\frac{\sigma_{\text{cr}}}{\sigma_{Y,S}} = \frac{\pi E_s}{16\sigma_{Y,S}}\left(\frac{\sigma_Y}{\sigma_{Y,S}}\right), \tag{48}$$

where $(\sigma_Y/\sigma_{Y,S})$ for a cube-based structure is given by Eq. (37). For the polylactic acid (PLA) material, E_s is around 40 times higher than $\sigma_{Y,S}$. In other words, buckling stress is 7.81 times the yield stress. Hence, yielding occurs before buckling.

B. Computational models

For FE modeling of beams with variable cross sections, 3D structures are modeled using 8-noded brick elements (SOLID185). ANSYS implicit FE solver is used. A linear elastic material model is used for predicting the response of the beams. Macro codes are written in ANSYS to automatically create, discretize, load, and obtain the required properties of beams with four different beam geometries and with different α ratios. An example of the 3D FE model of a single beam is presented in Fig. 3(a). One of the ends of each beam is fixed in the space, while the other end is displaced downward by applying a point load or moment.

For numerical modeling of the unit cells, 3D structures based on diamond and cube unit cells are created using

FIG. 3.   Two examples of the 3D FE models, which are used for evaluating the analytical solutions of the (a) single strut and (b) lattice structure.

8-noded brick elements (SOLID185). Macro codes are written to automatically create, discretize, load, and obtain the required properties of cubic or diamond unit cells with concave and convex double-cone struts. The lower face of the unit cell is fixed in the Y direction, while the top face is displaced downward to cause 0.2% compression. An example of the diamond-based unit cell with struts having the geometry of a convex double cone is presented in Fig. 3(b).

C. Experiments

Several specimens with diamond-based and cube-based unit cells are additively manufactured. Two (convex double cone and concave double cone) of the four beam types (convex double cone, concave double cone, convex hyperbolic, concave hyperbolic) are chosen for the experimental study. Lattice structures with three different micro-architectures are manufactured, cube-based lattice structures with concave double-cone struts and diamond-based lattice structures with either convex double-cone or
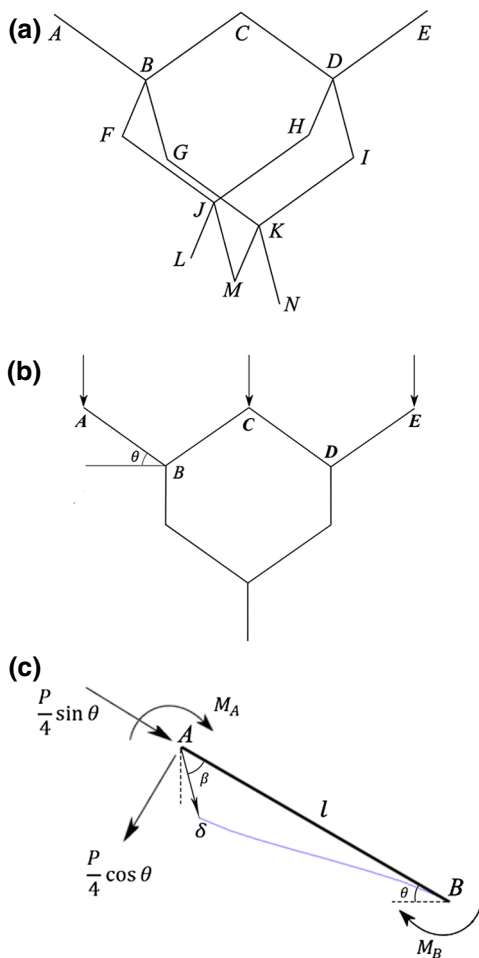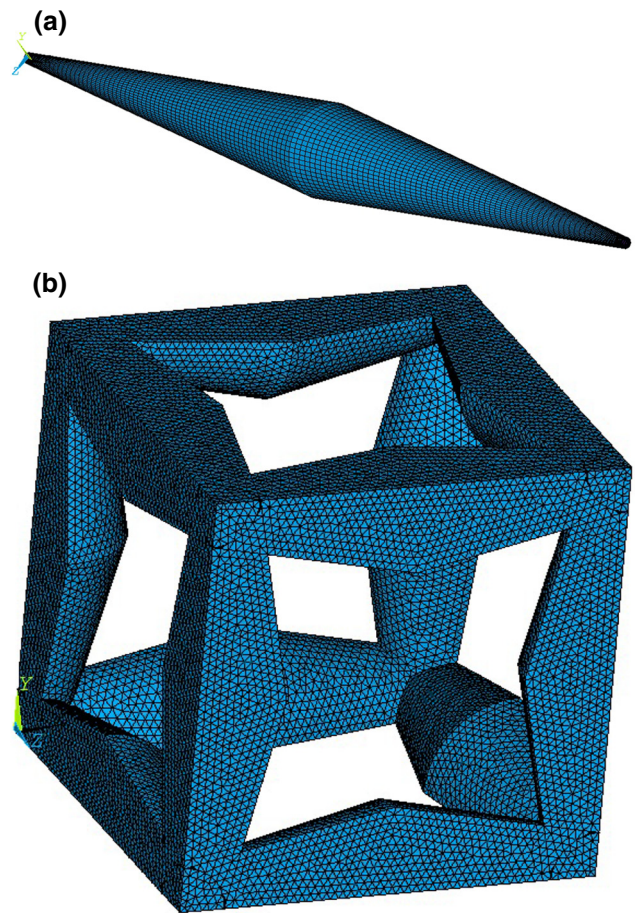
FIG. 2.   (a) A diamond cubic unit cell (b) the diamond cubic unit cell from front view, and (c) the loads transferred to strut AB and the resulting deformation.
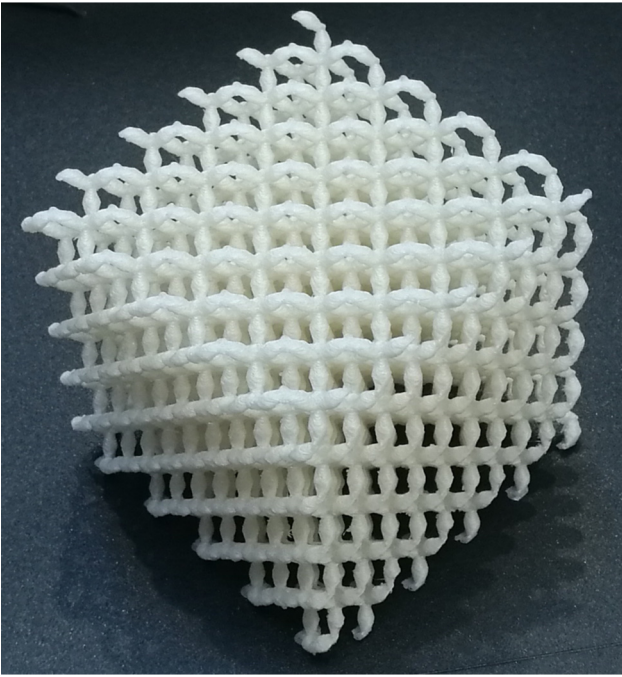
FIG. 4.   A pentamode metamaterial sample specimen ($\mu = 0.2$ and $\alpha = 2$).

concave double-cone struts. The cube-based lattice structures with convex double-cone struts are not manufactured due to reasons explained in the Results and Discussions sections. Among the three cases, specimens based on the diamond unit cell and with convex double-cone struts have the microstructure of a pentamode metamaterial (Fig. 4) [7,23,24,28,29]. The relative densities of the diamond-based lattice structure (with both concave and convex double-cone struts) and cube-based structure are varied between 0.1 and 0.4 at a constant α (=2) to study the effects of the relative density of the lattice structure on the elastic modulus of the resulting mechanical metamaterial. In another parametric study, the ratio α is varied between 1 and 4 to study the effects of the α value on the elastic modulus of the lattice structures (Fig. 5). The parametric study on α effect is done at a relative density of 0.1 for diamond-based structures and a relative density of 0.4 for cube-based structures. For each design of the lattice structure, three specimens are manufactured and tested under compression (66 specimens in total). The macrogeometry of all the specimens is a cube with dimensions of $8 \times 8 \times 8$ cm^3.

The samples are manufactured using Ultimaker 2+ 3D printers (Ultimaker, The Netherlands) that work on the basis of fused deposition modeling (FDM). PLA filaments with a pearl white color from the same provider are used. The infill in all the samples is set to 100% and the layer thickness is 200 μm. The static compression tests are performed using an INSTRON Electropulse E10000

machine with a 10-kN load cell. The compression tests are performed in accordance with ISO standard 13314:2011, which refers to the mechanical testing of porous and cellular materials. The displacement rate is fixed at 2 mm/min. The elastic modulus of the specimens is obtained by calculating the slope of the stress-strain curve in the linear part. Nonporous (i.e., fully solid) cylindrical samples are made and tested to obtain the mechanical properties of the bulk filament. The cylinders have diameters of 12.7 mm and lengths of 25.4 mm. The mean elastic modulus obtained for the pearl white filament is 1.404 GPa and the mean yield stress is 35.28 MPa.

III. RESULTS

A. Single beams with variable cross sections

1. Number of terms

In the analytical solution, the number of terms of δ_{lateral}, δ_{axial}, and θ [in Eq. (9)] is increased from $k = 2$ to $k = 16$ to see at what k the results of the analytical model converge. The solution converged for all geometries except the convex double cone for $k \cong 14$ (Fig. 5). The convex double-cone geometry converged at $k = 10$. It must be noted that by increasing the number of terms to values larger than $k = 14$, small pivots are formed in the stiffness matrix of the beams [i.e., in Eq. (17)] due to which the determinant of the stiffness matrix becomes very small, causing fluctuations in the curves [see, for example, the curve corresponding to $k = 12$ in Fig. 5(a)]. In each case, the converged curve (with the maximum number of terms before fluctuations are formed in the curve) is used for the semi-analytical study presented in the next sections.

2. Displacement curves

The lateral displacements resulting from the lateral force ($F_0 = 0.1$ N), the lateral displacements caused by the point moment ($M_0 = 0.002$ N m), and the axial displacements imposed by the axial load ($P_0 = 1000$ N) for different geometries and α ratios are presented in Fig. 6. For the cases of lateral force and moment loadings [Figs. 6(a) and 6(b)], the numerical and analytical results show a generally good agreement for all α values. The only exception is the concave double-cone geometry under moment loading for which there are larger discrepancies between the analytical and numerical solutions for α ratios larger than 3 [Fig. 6(b)]. For the case of axial loading, the numerical and analytical curves are very close for all the geometries [Fig. 6(c)]. As expected, the curves corresponding to different geometries coincide at $\alpha = 1$ (Fig. 6), that is, when the maximum and minimum radii are the same and all strut shapes reduce to cylinders ($r = R$).

Increasing the α ratio increases the resulting displacement in all the cases. For example, in the case of lateral force loading [Fig. 6(a)], the lateral displacements of both
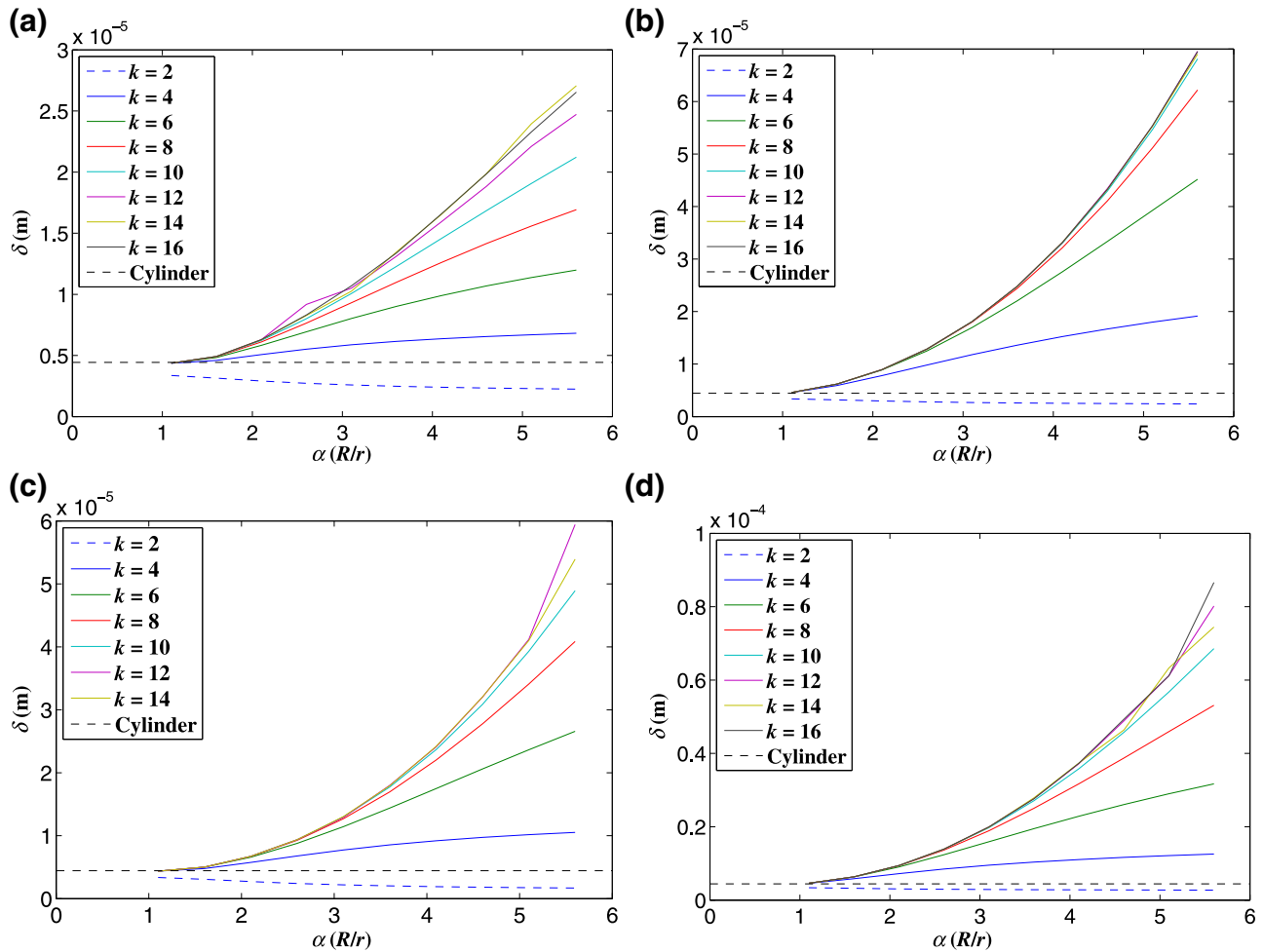
FIG. 5.   Effect of number of terms on the resulting lateral displacement at the free end of a cantilever beam with (a) concave double-cone, (b) convex double-cone, (c) concave hyperbolic, and (d) convex hyperbolic geometries.

the concave hyperbolic and concave double-cone geometries in $\alpha = 3$ are, respectively, around 2 and 4 times larger than that of the cylindrical geometry. Similar values are observed for the convex hyperbolic and convex double-cone geometries. In the case of point moment loading [Fig. 6(b)], at $\alpha = 3$, the lateral displacement of all the four geometries is about 3 times larger than of the cylindrical geometry. As for axial loading [Fig. 6(c)], all the geometries except for the concave hyperbolic geometry show similar behaviors. At $\alpha = 3$, for example, the extensions of the convex hyperbolic, concave double-cone, and convex double-cone geometries are about 1.45 times that of a simple cylinder. At $\alpha = 3$, the axial extension of the concave hyperbolic geometry is about 1.67 times the values found for a simple cylinder.

3. Normal stress distribution

The normal and shear stresses calculated for the outer fiber of the struts along the strut length for both loading

types of lateral force and moment are presented in Figs. 7 and 8, respectively. The analytical and numerical stresses practically overlap, which is why only the analytical results are plotted in Figs. 7 and 8. Under both lateral force and moment loads, the stress value is maximum at the center of beam for all the concave geometries (Fig. 7). The only exception is the concave hyperbolic geometry under lateral force [Fig. 7(c)]. Moreover, the normal stress distribution is symmetrical with respect to the center of the beams in all the beam geometries and loading conditions. The only exceptions are the convex geometries under lateral force, which show a maximum normal stress at $x = 0$ and a minimum normal stress at $x = l$ [Figs. 7(a) and 7(c)].

For beams with $\alpha = 6$ and under lateral force loading, the concave double-cone geometry shows the maximum normal stress (about 11 MPa) [Fig. 7(a)]. Again, for beams with $\alpha = 6$ under moment loading, the maximum normal stress belongs to both the concave and convex double-cone geometries (8.5 and 7 MPa, respectively) [Fig. 7(b)], while
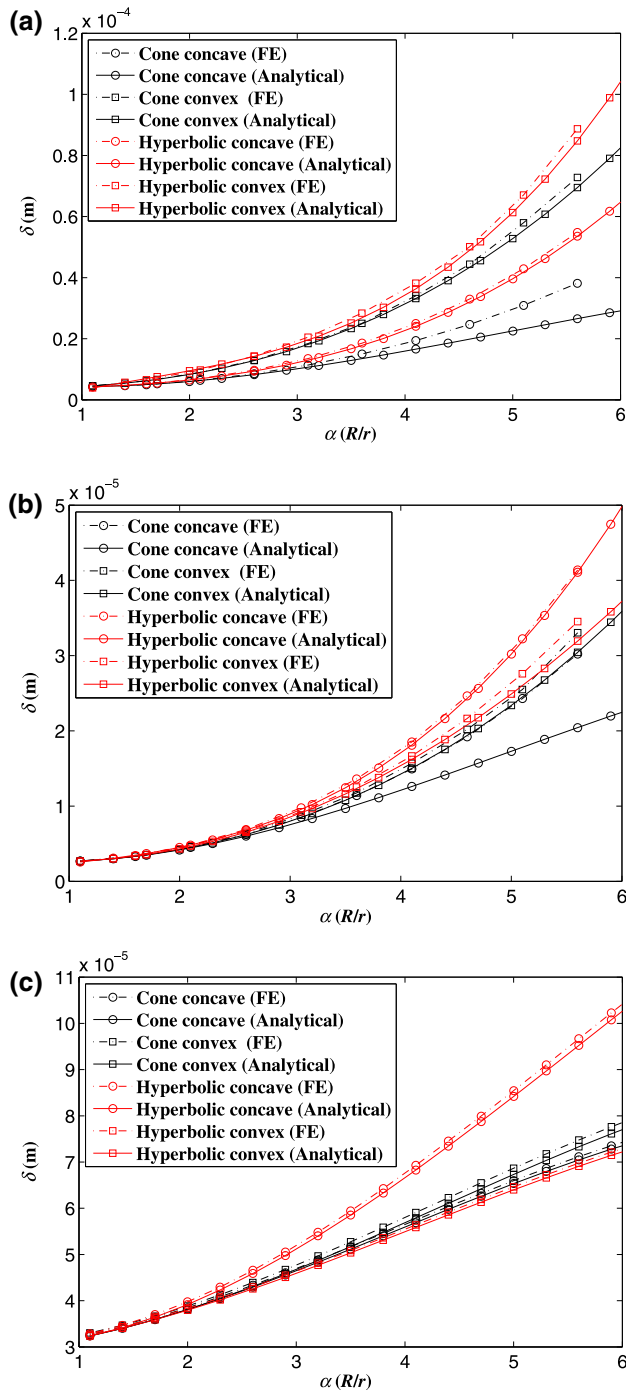
FIG. 6.   (a) Lateral displacement due to lateral force, (b) lateral displacement caused by point moment, and (c) axial displacement imposed by axial load for different geometries and α ratios in constant mass of the strut.

the maximum normal stress in the hyperbolic geometry is less than 3 MPa [Fig. 7(d)].

4. Shear stress distribution

The shear stress exhibits a somewhat different behavior (Fig. 8). The shear stress in the concave double-cone

geometry (under both lateral force and moment loads) is found to suddenly change in the middle of the strut from a negative value to a positive value with the same amplitude [Figs. 8(a) and 8(b)]. The concave hyperbolic geometry also shows the change of shear stress from a negative value to a positive value, but in a gradual way [Figs. 8(c) and 8(d)]. Under both lateral force and moment loadings, the maximum shear stress in the concave double-cone geometry is about 6 times of that in the concave hyperbolic geometry. Under lateral force loading, the maximum shear stress for the convex beams occurs at the clamped end of the beam [Figs. 8(a) and 8(c)], while under moment loading, the maximum shear stress for the same type of beams occurs at both the free and clamped ends of the beam (Fig. 8).

B. Mechanical metamaterials

Deformation: Under compression, all the diamond-based lattice structures show three-stage stress-strain curves. In the first stage, the curve is linear. After the stress level reaches a local maximum, it decreases to about half of the initial maximum value. In the second stage, the strain greatly increases with very small accumulations in the stress value (the stress at this stage is known as the plateau stress). In the final stage, the stress-strain curve also shows a second linear part (known as the densification regime). In all the diamond-based structures, after the stress reaches the initial maximum stress, 45° failure bands are formed (Fig. 9) after which the stress value is decreased to half the value of the initial maximum stress. In the cube-based structures, the structures fail after a row of unit cells are buckled and fractured without showing any 45° failure band. As a result, the cube-based structures do not show the plateau and densification parts in their stress-strain curves.

Elastic modulus: The effects of the relative density μ and α ratio on the relative elastic modulus of both diamond- (Fig. 10) and cube-based (Fig. 11) structures is also investigated. As expected, increasing the relative density, while keeping the α ratio ($\alpha = 2$) constant, increases the elastic modulus in both the diamond- and cube-based structures (Figs. 10–12). The numerical and analytical results are close, especially for small values of relative density [Figs. 10(a) and 10(b) and 11(a)]. The γ values that are obtained for Eq. (32) in such a way that analytical curves approach the experimental and numerical ones are presented in the titles of each plot in Fig. 10. The numerical and analytical results are less than 10% different even at relative densities as large as 30% (Figs. 10 and 11). As compared to the diamond-based structure, the cube-based structure shows a much higher elastic modulus. For example, at $\mu = 0.2$ and $\alpha = 2$, the elastic modulus of the structure with cubic unit cell is more than 8 times of that of the structure with the diamond-type unit cell.
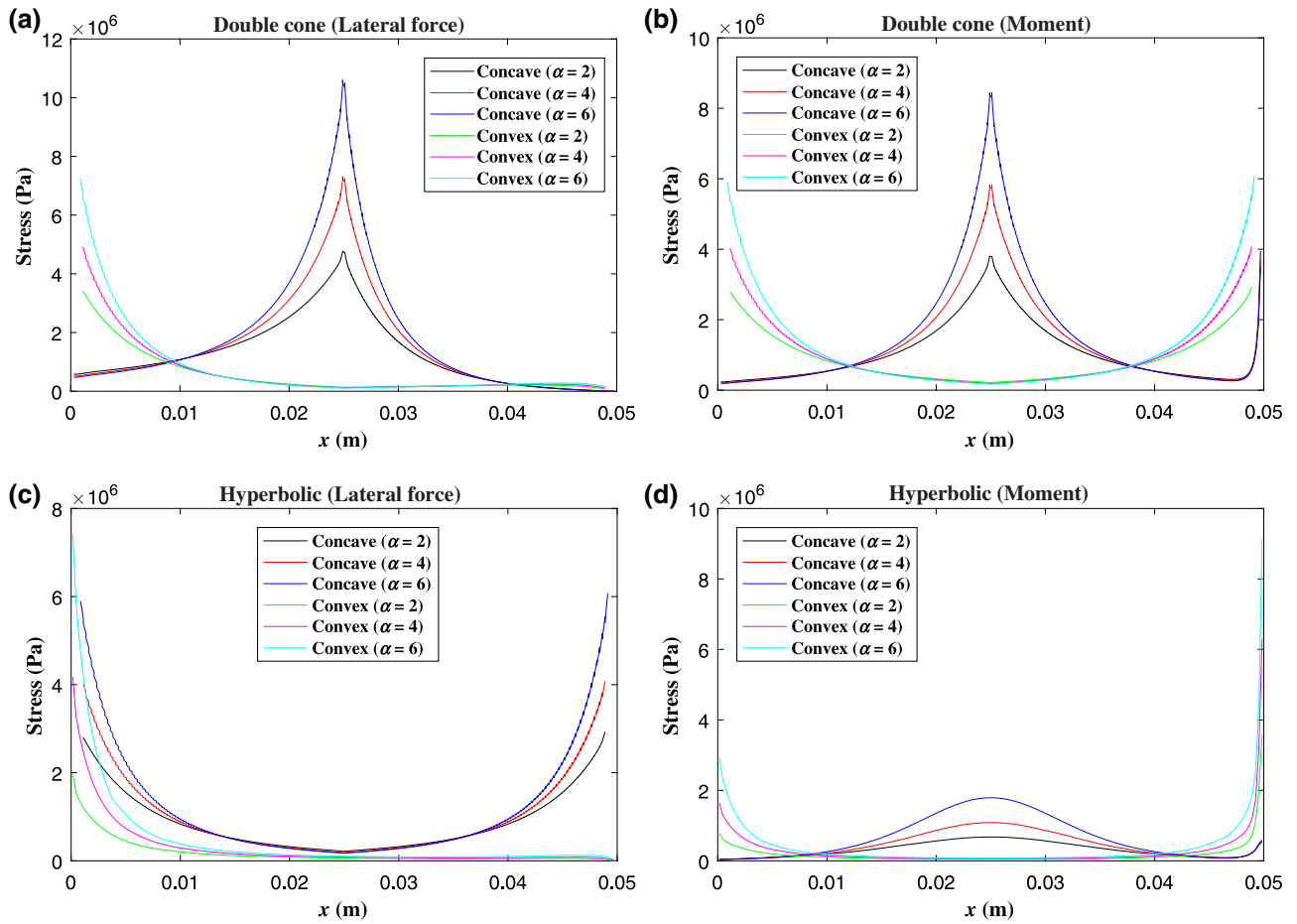
FIG. 7.   The normal stress value at the outer fiber of the cantilever beam for (a) double-cone geometries under lateral force, (b) double-cone geometries under moment, (c) hyperbolic geometries under lateral force, and (d) hyperbolic geometries under moment.

The effects of α value on the obtained elastic modulus values is more interesting, because the pentamode metamaterials investigated in this study are suggested as substitutes for currently used porous structures in which the strut cross-section areas are uniform. The effects of the α value are investigated at a constant relative density of $\mu = 0.1$ for the diamond-based lattice structure [Figs. 10(c) and 10(d)] and $\mu = 0.4$ for the cube-based lattice structures [Fig. 11(b)]. The analytical, numerical, and experimental results in both cube- and diamond-based structures are close [Figs. 10(c) and 10(d) and 11(b)]. In both the cube- and diamond-based structures, increasing the α value decreases the elastic modulus. As compared to the cube-based structures, increasing the α value has a higher impact on the elastic modulus of the diamond-based structures, especially at small values of α (i.e., more uniform struts). Increasing the α ratio from $\alpha = 1$ to $\alpha = 4$ decreases the analytically obtained elastic modulus of the diamond-based and cube-based structures (with convex double-cone struts) for, respectively, 92.24% (about 1/13) [Fig. 10(c)] and 44% (about half) [Fig. 11(b)].

Increasing the relative density of the diamond-based and cube-based lattice structures (with convex double-cone struts) from 0.1 to 0.3 increases the analytical relative elastic modulus by 636% [Fig. 10(a)] and 300% [Fig. 11(a)], respectively.

Yield stress: Since the maximum load applied by the compression test machine is 10 kN, among all the cube-based structures, only two cases of ($\mu = 0.1$ and $\alpha = 2$) and ($\mu = 0.4$ and $\alpha = 4$) yield. For the other cases, the experiment is ended before the lattice structures yield. The closed-form analytical and experimental yield stresses for the cube-based and pentamode diamond-based lattice structures are compared to each other in Fig. 12. Similar trends to that observed for the elastic modulus curves is observed for the yield stress. In other words, increasing the relative density at constant α ratio ($\alpha = 2$) increases the relative yield strength, and increasing the α ratio at a constant relative density ($\mu = 0.1$ for a diamond-based structure and $\mu = 0.4$ for a cube-based structure) decreases the relative yield strength. For the diamond-based structure, there is a good agreement between the analytical and
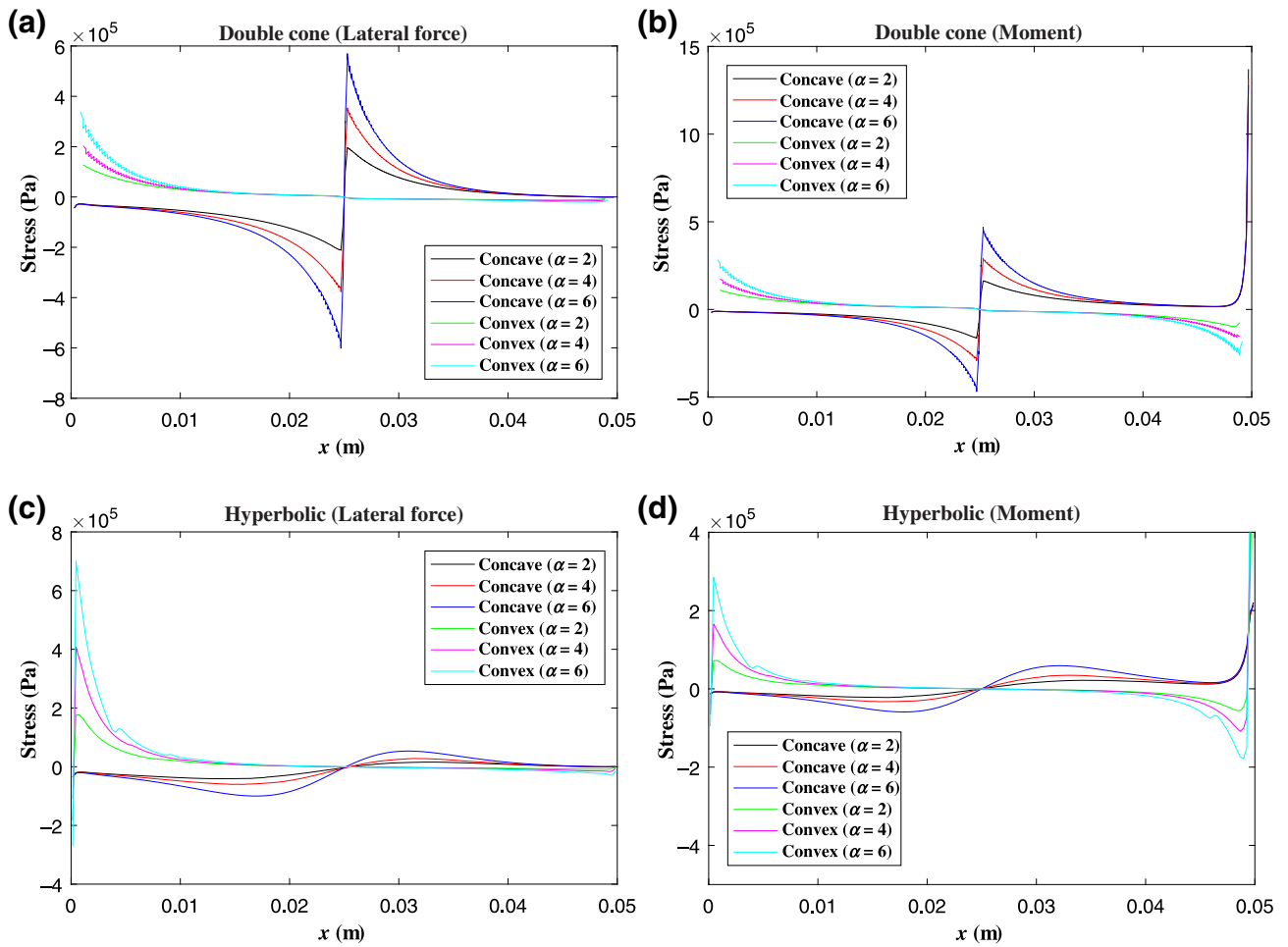
FIG. 8. The shear stress value at the outer fiber of the cantilever beam for (a) double-cone geometries under lateral force, (b) double-cone geometries under moment, (c) hyperbolic geometries under lateral force, and (d) hyperbolic geometries under moment.

experimental results. For the cube-based structure with $\mu = 0.1$ and $\alpha = 2$, the measured experimental relative yield stress is much lower than the value predicted by the analytical relationships. As is also confirmed by experiments, this can be due to the fact that at very low values of the relative density (i.e., $\mu = 0.1$), due to irregularities in the cross-section area, buckling occurs much earlier than what is predicted analytically. In other words, the absolute size of the manufacturing irregularities (i.e., variations in the dimensions of the cross section of the struts) is similar regardless of the relative density. However, in low relative densities, the relative importance of the manufacturing irregularities is much higher than when the relative density, and thus, the dimensions of the cross section are much higher.

IV. DISCUSSIONS

The results show that for constant mass, increasing the α ratio in beams with variable cross sections increases the maximum normal stress (Fig. 7), maximum shear

stress (Fig. 8), and the lateral displacement at the free end of the cantilever beam (Fig. 6). Therefore, a 3D lattice structure with struts having a variable cross section
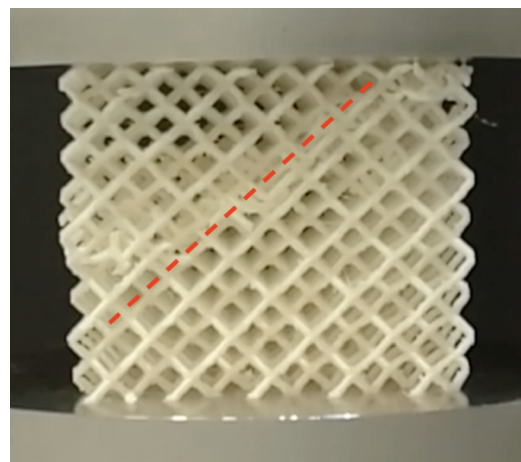

FIG. 9. Formation of 45° deformation bands in pentamode metamaterial (The failure bands are marked by red lines.).
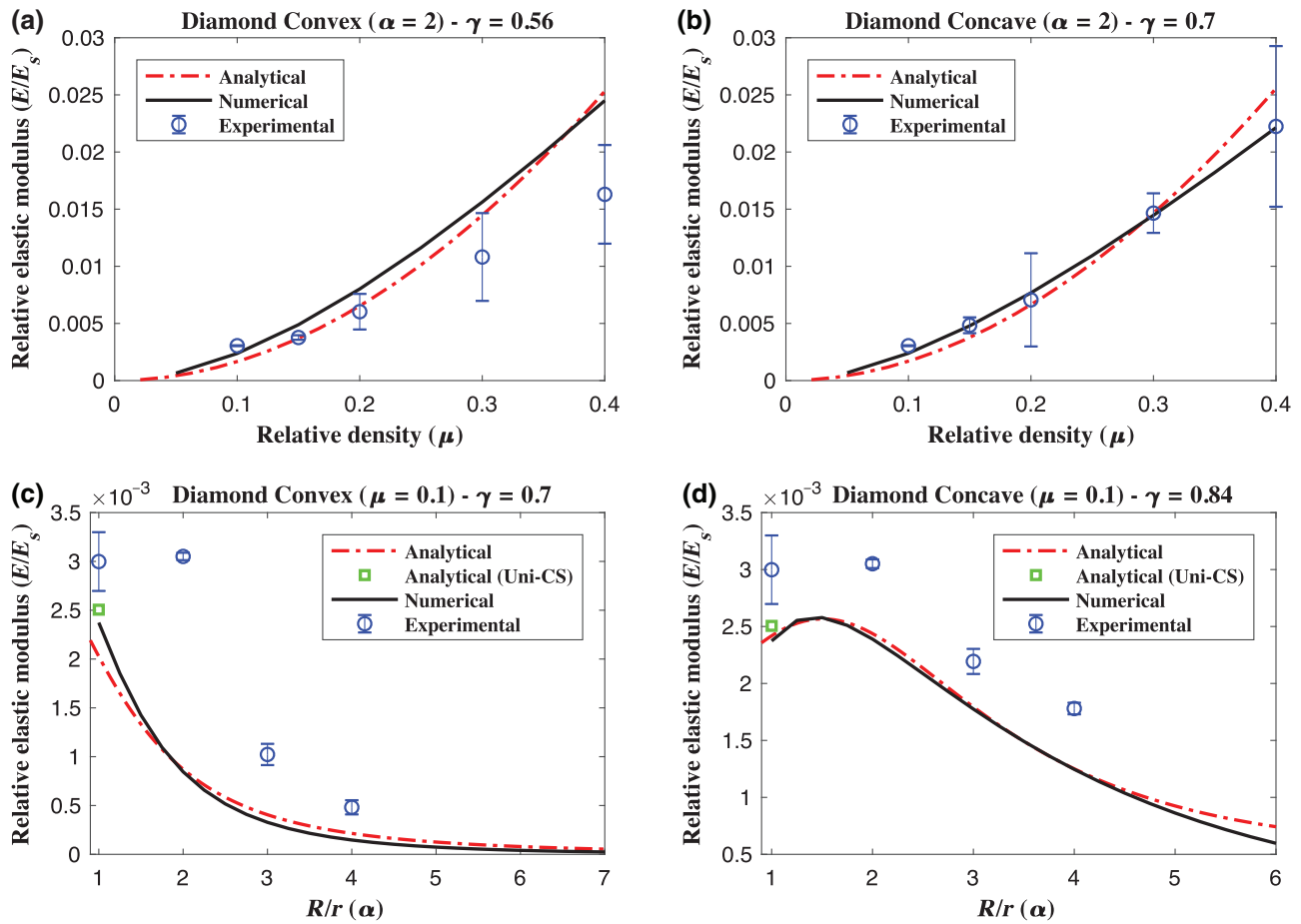
FIG. 10.   Effect of relative density on the relative elastic modulus of diamond pentamode structures with (a) convex and (b) concave double-cone struts and constant α ratio ($\alpha = 2$). Effect of α ratio on the relative elastic modulus of diamond pentamode structures with (c) convex and (d) concave double-cone struts and constant relative density ($\mu = 0.1$). The γ value used for each case is shown in the title of each plot.

is probably more susceptible to failure under external forces as compared to a lattice structure with uniform cross-section area and similar mass. As a good example of such structures, 3D pentamode metamaterial lattice structures (with struts having convex double-cone geometry) as well as two other pentamode-like lattice structures (diamond-based structures with concave double cones and cube-based lattice structures with concave double cones) are manufactured and tested. The anticipated behavior is observed in the 3D structures as well. There are two main manufacturing limitations that must be considered in such structures. First, although it is possible to additively manufacture diamond-based structures with convex double cones, it is not possible to additively manufacture cube-based structures with convex double cones without use of internal support bridges. This is because in the horizontal struts of the cube-based lattice structures with convex double cone, the part with the maximum diameter is printed first. Since that

part is not supported by previously printed layers, that layer falls down. Other manufacturing techniques such as multimaterial additive manufacturing techniques with water-soluble support material or a powder-bed diffusion technique do not have such limitations, since the easily removable support material holds the initially printed large-diameter parts of the horizontal struts. The other problem associated with the FDM technique in manufacturing of pentamode and pentamode-like structures is that when the cross-section area of the struts is very small, the quality of the print severely decreases, and several pores are created in the part with the lower diameter.

It has been shown in previous studies [24,28,29] that the elastic modulus of very low-density pentamode metamaterials (with convex double cones) are independent from their relative density and the maximum diameter of the struts, and the elastic modulus is only dependent on the diameter of the touching region in the
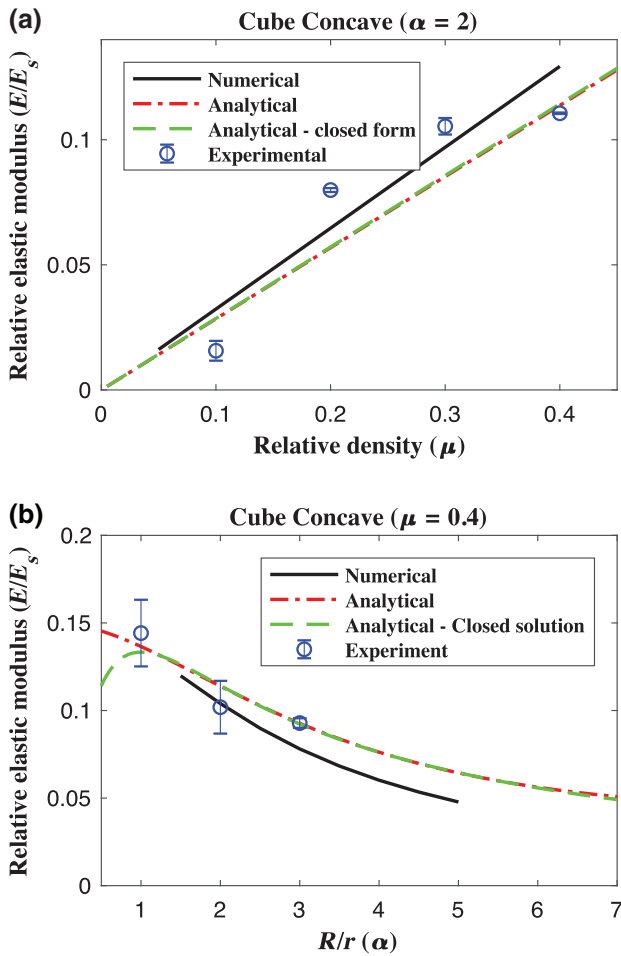
(a)

(b)

FIG. 11. (a) Effect of relative density on the relative elastic modulus of cube-based structures with concave double-cone struts and constant α ratio ($\alpha = 2$). (b) Effect of α ratio on the relative elastic modulus of cube-based structures with concave double-cone struts and constant relative density ($\mu = 0.4$).

vertices [29]. The pentamode metamaterials manufactured and studied here have relative densities larger than 0.1. Due to the limitations of the FDM technique, mechanical materials with very small relative densities cannot be manufactured. Studying the noted statement using the analytical relationships obtained in this paper is also not possible since our analytical relationships are functions of the small diameter of the struts $d = 2r$ and not the diameter of the struts at the touching region $d_t = 2r_t$. Using other additive manufacturing techniques, manufacturing very low-density pentamode metamaterials is feasible. For example, in our other study [7], several Ti-6Al-4V pentamode metamaterials with different relative densities (between 0.84% and 2.24%), but with the same touching region diameter, were made and tested under compression. The test results

demonstrated their very close elastic modulus and yield stress.

The analytical solutions obtained for struts with variable cross sections are used for obtaining the semi-analytical relationships for pentamode and pentamode-like mechanical metamaterials. The relationships obtained for other types of struts [Eq. (20) along with Table II] can also be used for obtaining semi-analytical relationships for the structures having other strut types as well as with other unit cell types, such as cube [30,31], rhombic dodecahedron [19,32], truncated cube [33], diamond [27], tetrakaidecahedrons [15,34], rhombicuboctahedron [18], and truncated cuboctahedron [20]).

The analytical and numerical results obtained in this study show that among the five proposed strut geometries having the same volume, the highest displacements belong to convex hyperbolic under lateral force and concave hyperbolic under axial force and point moment (Figs. 6 and 8). This suggests that the hyperbolic strut types are usually less stiff than double-cone struts. Moreover, in all loading cases, the concave double-cone geometry exhibits some of the lowest values of displacement. Therefore, it seems that structures having concave double-cone struts are the stiffest among the structures with the same unit cell type, but with other strut types. This is partly shown in the diamond-based lattice structures with concave and convex double cones [compare Figs. 10(a) and 10(b), compare Figs. 10(c) and 10(d)]. For future studies, it is suggested that the mechanical properties of mechanical metamaterials with the same unit cell types but with different strut types be compared with each other to see which structures have the highest stiffness, strength, and energy absorption capacities.

One of the recent important applications of 3D lattice structures is their use as bone-substituting biomaterials. In bone-substituting biomaterials, the stiffness of the implant is of great importance. If the stiffness of the implant is much larger than that of natural bones, it transfers most of the loads applied to the implanted bone and unloads the natural bone (the stress-shielding phenomenon). As a result, after a while, bone resorption occurs, leading to implant loosening. Therefore, it has been suggested to manufacture implants with stiffness distribution similar to the natural bone [35,36]. Lattice structures with various types of nonuniform cross sections could be used to mimic the spatial distribution of the mechanical properties of the bone tissue, while satisfying other important design requirements [37] such as pore shape [38], curvature [39], and permeability [40]. Using the same unit cell type throughout the implant while changing the cross section design has the advantage that connectivity between the various unit cells is straightforward. That is not the case when different types of unit cells have to be used in order to mimic the spatial distribution of the mechanical properties of the bone tissue.
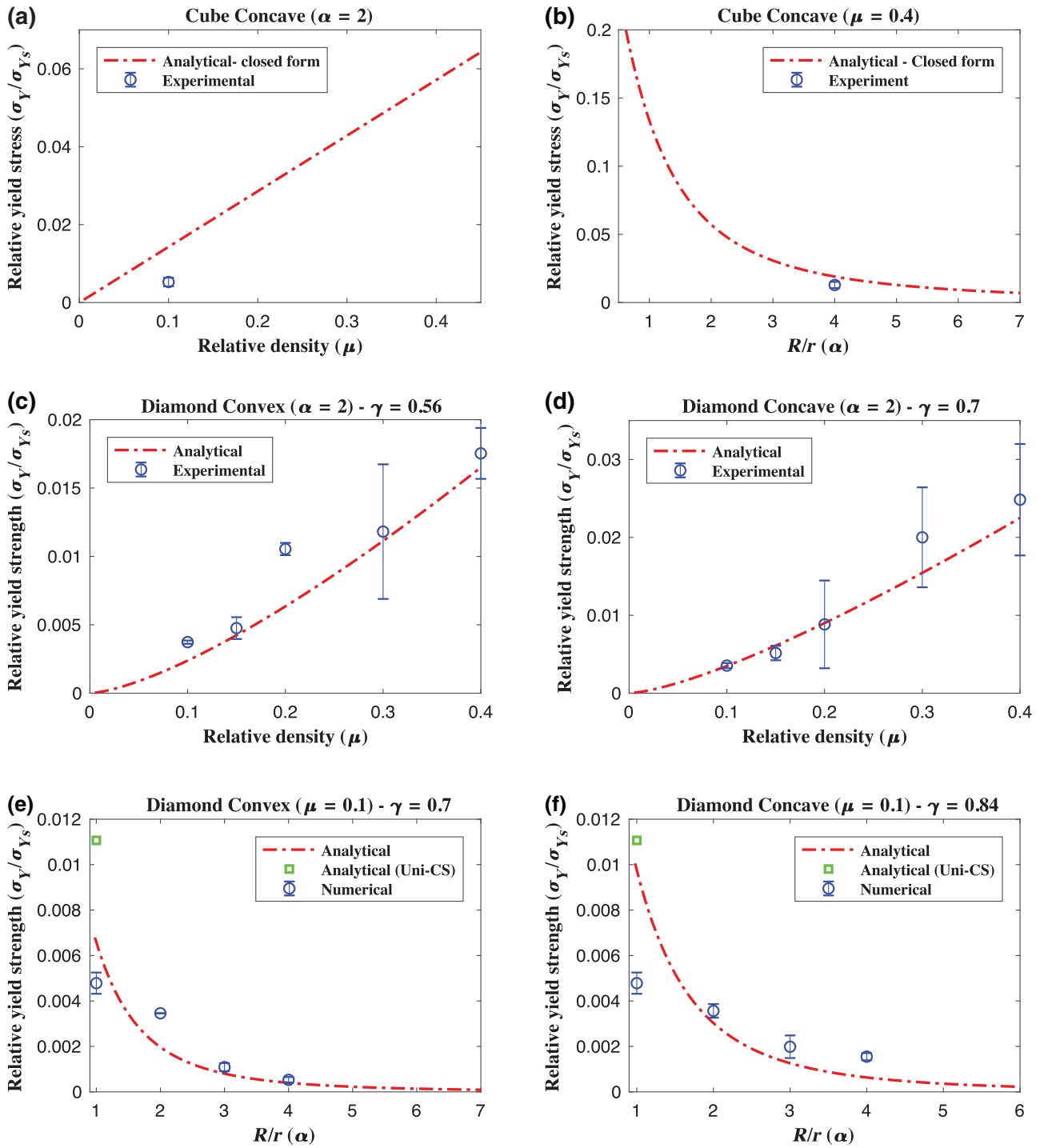
FIG. 12. The effects of relative density and α ratio on the relative yield strength for (a-b) cubic, and (c-f) diamond pentamode structures.

V. CONCLUSIONS

In this study, five different types of symmetrical struts, namely simple cylinder, concave double cone, convex double cone, concave hyperbolic, and convex hyperbolic, are considered. We then derive semi-analytical relationships to describe the mechanical response of the beams and lattice structures (diamond-type, cube-type) based on the above-mentioned types of cross sections. Comparison of the analytical, numerical, and experimental results demonstrate the accuracy of the semi-analytical relationships presented for the elastic modulus and yield strength of

these biomaterials. In both cube- and diamond-based structures, increasing the α value at constant relative density decreases the elastic modulus and yield strength.

———————

[1] J. Valentine, S. Zhang, T. Zentgraf, E. Ulin-Avila, D. A. Genov, G. Bartal, and X. Zhang, Three-dimensional optical metamaterial with a negative refractive index, Nature **455,** 376 (2008).

[2] Y. Zhao, M. Belkin, and A. Alù, Twisted optical metamaterials for planarized ultrathin broadband circular polarizers, Nat. Commun. **3,** 870 (2012).

[3] D. Torrent and J. Sánchez-Dehesa, Acoustic metamaterials for new two-dimensional sonic devices, New J. Phys. **9,** 323 (2007).

[4] H. Chen and C. Chan, Acoustic cloaking in three dimensions using acoustic metamaterials, Appl. Phys. Lett. **91,** 183518 (2007).

[5] A. A. Zadpoor, Mechanical meta-materials, Mater. Horiz. **3,** 371 (2016).

[6] J. H. Lee, J. P. Singer, and E. L. Thomas, Micro-/nanostructured mechanical metamaterials, Adv. Mater. **24,** 4782 (2012).

[7] R. Hedayati, A. Leeflang, and A. Zadpoor, Additively manufactured metallic pentamode meta-materials, Appl. Phys. Lett. **110,** 091905 (2017).

[8] R. Hedayati, M. Mirzaali, L. Vergani, and A. Zadpoor, Action-at-a-distance metamaterials: Distributed local actuation through far-field global forces, APL Mater. **6,** 036101 (2018).

[9] K. E. Evans and A. Alderson, Auxetic materials: functional materials and structures from lateral thinking!, Adv. Mater. **12,** 617 (2000).

[10] R. Gatt, L. Mizzi, J. I. Azzopardi, K. M. Azzopardi, D. Attard, A. Casha, J. Briffa, and J. N. Grima, Hierarchical auxetic mechanical metamaterials, Sci. Rep. **5,** 8395 (2015).

[11] H. M. Kolken, S. Janbaz, S. M. Leeflang, K. Lietaert, H. H. Weinans, and A. A. Zadpoor, Rationally designed meta-implants: a combination of auxetic and conventional meta-biomaterials, Mater. Horiz. **5,** 28 (2018).

[12] M. Mirzaali, R. Hedayati, P. Vena, L. Vergani, M. Strano, and A. Zadpoor, Rational design of soft mechanical meta-materials: Independent tailoring of elastic properties with randomness, Appl. Phys. Lett. **111,** 051903 (2017).

[13] R. Lakes and K. Wojciechowski, Negative compressibility, negative Poisson's ratio, and stability, Phys. Status Solidi B **245,** 545 (2008).

[14] Z. G. Nicolaou and A. E. Motter, Mechanical metamaterials with negative compressibility transitions, Nat. Mater. **11,** 608 (2012).

[15] X. Zheng, H. Lee, T. H. Weisgraber, M. Shusteff, J. DeOtte, E. B. Duoss, J. D. Kuntz, M. M. Biener, Q. Ge, J. A. Jackson, S. O. Kucheyev, N. X. Fang, and C. M. Spadaccini, Ultralight, ultrastiff mechanical metamaterials, Science **344,** 1373 (2014).

[16] R. Lakes and W. Drugan, Dramatically stiffer elastic composite materials due to a negative stiffness phase?, J. Mech. Phys. Solids **50,** 979 (2002).

[17] R. S. Lakes, T. Lee, A. Bersie, and Y. Wang, Extreme damping in composite materials with negative-stiffness inclusions, Nature **410,** 565 (2001).

[18] R. Hedayati, M. Sadighi, M. Mohammadi-Aghdam, and A. A. Zadpoor, Mechanics of additively manufactured porous biomaterials based on the rhombicuboctahedron unit cell, J. Mech. Behav. Biomed. Mater. **53,** 272 (2016).

[19] S. Babaee, B. H. Jahromi, A. Ajdari, H. Nayeb-Hashemi, and A. Vaziri, Mechanical properties of open-cell rhombic dodecahedron cellular structures, Acta Mater. **60,** 2873 (2012).

[20] R. Hedayati, M. Sadighi, M. Mohammadi-Aghdam, and A. Zadpoor, Mechanical behavior of additively manufactured porous biomaterials made from truncated cuboctahedron unit cells, Int. J. Mech. Sci. **106,** 19 (2016).

[21] G. W. Milton and A. V. Cherkaev, Which elasticity tensors are realizable?, J. Eng. Mater. Technol. **117,** 483 (1995).

[22] A. N. Norris, Acoustic metafluids, J. Acoust. Soc. Am. **125,** 839 (2009).

[23] C. N. Layman, C. J. Naify, T. P. Martin, D. C. Calvo, and G. J. Orris, Highly Anisotropic Elements for Acoustic Pentamode Applications, Phys. Rev. Lett. **111,** 024302 (2013).

[24] M. Kadic, T. Bückmann, N. Stenger, M. Thiel, and M. Wegener, On the practicability of pentamode mechanical metamaterials, Appl. Phys. Lett. **100,** 191901 (2012).

[25] See Supplemental Material at http://link.aps.org/supplemental/10.1103/PhysRevApplied.11.034057 for steps required to derive the factors C in Eq. (20).

[26] R. Wauthle, B. Vrancken, B. Beynaerts, K. Jorissen, J. Schrooten, J.-P. Kruth, and J. Van Humbeeck, Effects of build orientation and heat treatment on the microstructure and mechanical properties of selective laser melted Ti₆Al₄V lattice structures, Addit. Manuf. **5,** 77 (2015).

[27] S. Ahmadi, G. Campoli, S. Amin Yavari, B. Sajadi, R. Wauthlé, J. Schrooten, H. Weinans, and A. A. Zadpoor, Mechanical behavior of regular open-cell porous biomaterials made of diamond lattice unit cells, J. Mech. Behav. Biomed. Mater. **34,** 106 (2014).

[28] M. Kadic, T. Bückmann, R. Schittny, P. Gumbsch, and M. Wegener, Pentamode Metamaterials With Independently Tailored Bulk Modulus and Mass Density, Phys. Rev. Appl. **2,** 054007 (2014).

[29] R. Schittny, T. Bückmann, M. Kadic, and M. Wegener, Elastic measurements on macroscopic three-dimensional pentamode metamaterials, Appl. Phys. Lett. **103,** 231905 (2013).

[30] J. Parthasarathy, B. Starly, S. Raman, and A. Christensen, Mechanical evaluation of porous titanium (Ti₆Al₄V) structures with electron beam melting (EBM), J. Mech. Behav. Biomed. Mater. **3,** 249 (2010).

[31] L. J. Gibson and M. F. Ashby, *Cellular Solids: Structure and Properties* (Cambridge University Press, Cambridge, 1997).

[32] R. Hedayati, M. Sadighi, M. Mohammadi-Aghdam, and A. A. Zadpoor, Computational prediction of the fatigue behavior of additively manufactured porous metallic biomaterials, Int. J. Fatigue **84,** 67 (2016).

[33] R. Hedayati, M. Sadighi, M. Mohammadi-Aghdam, and A. A. Zadpoor, Mechanical properties of regular porous

biomaterials made from truncated cube repeating unit cells: Analytical solutions and computational models, Mater. Sci. Eng. C **60**, 163 (2016).

[34] W. Warren and A. Kraynik, Linear elastic behavior of a low-density Kelvin foam with open cells, J. Appl. Mech. **64**, 787 (1997).

[35] F. Bobbert, K. Lietaert, A. A. Eftekhari, B. Pouran, S. Ahmadi, H. Weinans, and A. Zadpoor, Additively manufactured metallic porous biomaterials based on minimal surfaces: A unique combination of topological, mechanical, and mass transport properties, Acta Biomater. **53**, 572 (2017).

[36] A. A. Zadpoor and J. Malda, Additive manufacturing of biomaterials, tissues, and organs, Ann. Biomed. Eng. **45**, 1 (2017).

[37] X. Wang, S. Xu, S. Zhou, W. Xu, M. Leary, P. Choong, M. Qian, M. Brandt, and Y. M. Xie, Topological design and additive manufacturing of porous metals for bone scaffolds and orthopaedic implants: a review, Biomaterials **83**, 127 (2016).

[38] R. Hedayati, S. M. Ahmadi, K. Lietaert, B. Pouran, Y. Li, Harrie Weinans, C. D. Rans, and A. A. Zadpoor, Isolated and modulated effects of topology and material type on the mechanical properties of additively manufactured porous biomaterials, J. Mech. Behav. Biomed. Mater. **79**, 254 (2018).

[39] A. A. Zadpoor, Bone tissue regeneration: the role of scaffold geometry, Biomater. Sci. **3**, 231 (2015).

[40] S. Van Bael, Y. C. Chai, S. Truscello, M. Moesen, G. Kerckhofs, H. Van Oosterwyck, J.-P. Kruth, and J. Schrooten, The effect of pore geometry on the in vitro biological behavior of human periosteum-derived cells seeded on selective laser-melted Ti_6Al_4V bone scaffolds, Acta Biomater. **8**, 2824 (2012).